NOVEL APPROACH FOR SELECTIVE DECOMPOSITION OF

TARGET WATER CONTAMINANTS ONTO POROUS

TITANIUM DIOXIDE

by

ABOLFAZL ZAKERSALEHI

Presented to the Faculty of the Graduate School of

The University of Texas at Arlington in Partial Fulfillment

of the Requirements for the Degree of

DOCTOR OF PHILOSOPHY

THE UNIVERSITY OF TEXAS AT ARLINGTON

December 2016

Acknowledgements

December 15, 2016

Abstract

NOVEL APPROACH FOR SELECTIVE DECOMPOSITION OF TARGET

WATER CONTAMINANTS ONTO POROUS TITANIUM DIOXIDE

Abolfazl Zakersalehi, PhD

The University of Texas at Arlington, 2016

Hyeok Choi

Manipulation of physical and chemical properties of matter with nanoscale precision will enhance our ability for fabrication of material with intended characteristics for environmental applications. In this study we presented two main frameworks for addressing non-selectivity issue in TiO_2 photocatalysts, which is believed to be a major drawback in full-scale application of this technology. First, a purely physical approach for enhancing selectivity of nanostructured TiO_2 photocatalysts toward water target contaminants have been achieved via tailor-designing meso-porous structure of TiO_2. This simple, yet effective method is mainly based on size-exclusion as a mean toward preferential decomposition. It was hypothesized controlled mesoporous structure of TiO_2 is capable of providing reaction sites for target contaminants while suppressing the access of large-size competing chemicals. Size-sensitivity of this method was evaluated by changing the size range of target contaminants from 1nm (Ibuprofen) to 1.7 nm (Methylene Blue) to 3nm (Microcystin-LR) combined with Humic Acid (HA) as model NOM. In agreement with proposed hypothesize; along with decrease in molecular size of target contaminants, better selectivity was accomplished. Changing the size of HA

species proved to affect the selectivity in both porous and non-porous TiO_2 particles. Largest size fraction of HA showed the highest selectivity enhancement using porous TiO_2 implying the exclusion of competing HA based on physical separation. In agreement with proposed adsorption model, the role of inter-porous structure proved to be more significant in cases with more limitation in surface area i.e. lower catalyst to target contaminants concentration. The role of medium pH as a major contributor to TiO_2 surface charge was evaluated in latter part of this study. It was observed, the effect of pH-induced surface charge was significant in terms of adsorption as well as decomposition of ionic organic species. The adsorption behavior shows clear pattern in accordance with ionization state of target contaminant as well as TiO_2 surface charge. This proved to be especially efficient in combination with proposed size-exclusion, resulting in considerable recovery in selectivity. From a technical point of view, this study provides basis for designing the physiochemical properties of photocatalysts as well as the reaction conditions for enhanced selective decomposition of target contaminants.

Table of Contents

List of Illustrations

List of Tables

CHAPTER 1

Introduction

1.1. Advanced Oxidation Technologies and TiO_2 Photocatalysis

Along with rapid industrialization, urbanization and population growth, a tremendous quantity of synthetic organic chemicals is produced and discharged directly or indirectly into natural resources. The variety and chemical stability of many of these contaminants has proven to be a major concern in environmental sectors since natural remediation and conventional treatment methods suffer from effective removal of many of these contaminants. In particular, the increasing occurrence of Emerging Chemicals of Concern (CECs) including pharmaceuticals and personal care products (PPCPs) in environment evidences the inability of conventional wastewater treatments in efficient removal of this class of contaminants (Maruya et al. 2016). As a result, a great amount of research has been devoted to develop and utilize novel physiochemical methods for removal and destruction of these contaminants. Among alternatives, advanced oxidation technologies (AOTs) are given special attention since these processes are capable of complete mineralization of contaminants into harmless compounds such as CO_2 and NO_2 and H_2O and other inert compounds (Deng & Zhao 2015).

AOTs (also referred as advanced oxidation processes) are a group of chemical reactions for destruction of organic compounds (sometimes inorganic compounds). They are generally initiated by generation of hydroxyl radicals ($^{\cdot}OH$), produced by various chemical routes. Among AOTs, Nanocrystalline TiO_2 has demonstrated promising properties for water treatment applications. In addition to its capability to decompose any organic contaminant, new generations of TiO_2-based processed are characterized by green properties such as non-toxicity, photo-stability and solar-activation, making it one of the most important semiconductor materials for environmental applications (Park et al. 2016). However, low "practical" activity of TiO_2-based processes results in higher operating cost to this technology, inhibiting it from being implemented in full-scale. In this regards, the effective activity of TiO_2 needs to be significantly improved before it can compete with current treatment alternatives. During last two decades an extensive amount of research has been conducted to increase pure activity of TiO_2 photocatalysts. This implies TiO_2 photocatalysts are capable of better light to hydroxyl radical conversion, resulting in larger overall kinetics. Reactivity enhancement is certainly beneficial; nevertheless when we

2

are dealing with a mixture of organic species in reaction medium, a distinct line can be drawn between *reactivity* and *selectivity*.

1.2. Challenges Facing TiO$_2$ photocatalysis

Decontamination of water using TiO$_2$ photocatalysis process is predominantly initiated by generation of highly reactive hydroxyl radicals ($^\bullet$OH) which can readily and non-selectively attack organic contaminants. As shown in Figure 1.1., the process is initiated by UV (in some cases solar spectrum) irradiation followed by excitation of electron from valance band to conduction band in TiO$_2$ semiconductor.
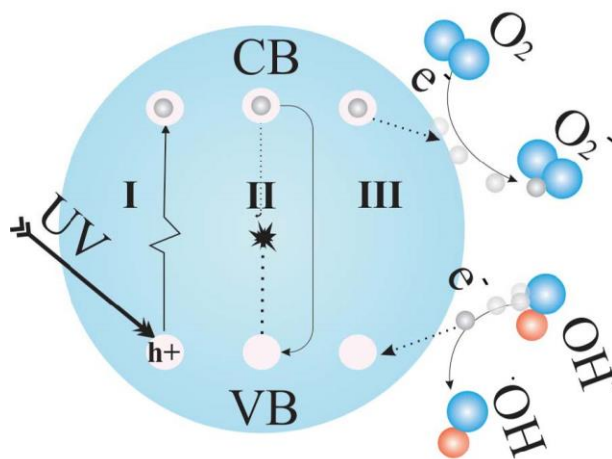
Figure 1.1. Schematic demonstrating the photocatalytic generation of reactive radical species in a TiO$_2$/UV system.

The reaction steps: (I) UV light irradiation to TiO$_2$ surface, electron excitation from the valence band (VB) to the conduction band (CB), and generation of electron (e$^-$) and hole (h$^+$) pairs; (II) recombination of the electrons and holes; and (III) formation of reactive radicals by redox reactions on TiO$_2$ surface.

The generation of reactive radicals takes place through following pathways:

(i) $O_2 + e^- \longrightarrow O_2^-$ *Equation 1.1.*

(ii) $OH^- + h^+ \longrightarrow {}^\bullet OH$

3
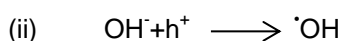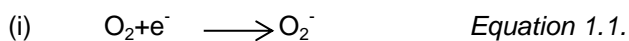
The generated OH attack organic molecules by one of the following pathways: I) electrophilic addition as shown in Equation 1.2.. II) Hydrogen atom abstraction, Equation 1.3. III) Electron transfer, Equation 1.4.. The hydroxyl radical additions to carbon–carbon double bonds and electron-rich aromatic systems leading to hydroxylated adducts are generally faster than H-abstraction and electron transfer reactions. Electron transfer with hydroxyl radical takes place only in electron rich systems.

$$RHC=CR2 + {}^{\bullet}OH \rightarrow RHC(OH)-C({}^{\bullet})R2 \qquad \textit{Equation 1.2.}$$

$$R3C-H + {}^{\bullet}OH \rightarrow R_3C({}^{\bullet}) + H_2O \qquad \textit{Equation 1.3.}$$

$$RH + {}^{\bullet}OH \rightarrow R^{\bullet} + H_2O \qquad \textit{Equation 1.4.}$$
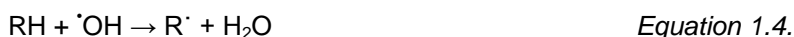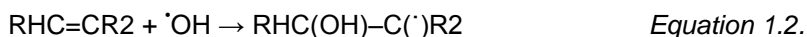
The reaction rate constant of generated ${}^{\bullet}OH$ reaction with organic molecules is in the range of 10^6–10^{10} $M^{-1}\,s^{-1}$ representing instant reaction with most organic compounds . As a result, TiO_2 photocatalysis is characterized with non-selective attack (Lazar and Daoud, 2013; Kavurmaci and Bekbolet, 2014; Rasoulifard et al., 2014). The non-selectivity of the process implies that it works versatilely even for a mixture of various organic chemicals. However, the non-selectivity is problematic especially when less (non-) toxic chemicals are co-present with toxic chemicals as targets to decompose (Paz, 2006). Photocatalytic oxidation should focus on decomposition of toxic targets. During the photocatalytic reaction non-targets as competing chemicals are also decomposed, the intended oxidation capability of TiO_2 photocatalysis is diluted, resulting in significant reduction in decomposition rate of target contaminants (Autin et al., 2009). This situation becomes critical under practical water treatment scenarios where most of water resources contain naturally abundant organic components, i.e., natural organic matter (NOM), which are in general not toxic or they can be removed inexpensively with other methods (Volk et al., 2002; Richardson and Ternes, 2014). Concurrent decomposition of NOM with targets implies that higher energy input and longer treatment time are required to achieve a desired level of treatment. Consequently, enhancing selective decomposition of target contaminants is an urgent interest in TiO_2-based water treatment, which has not been properly highlighted in previous studies.

4

1.3. Current Understanding and Research Need

The adverse effect of nonselective reaction route is well known issue in the field catalysis. Reaction of non-selective reactants not only causes lower kinetic for designated reaction, it also can result in formation of products that are chemically unfordable, lowering the quality of end products. Similarly, in photocatalysis of toxic target contaminants it is general understanding that presence of competing NOM will result in significant decline in decomposition rate of target contaminant since a great portion of energy input is wasted in decomposition of NOM (which can be easily and inexpensively removed by coagulation and filtration process(Matilainena et al 2010). Despite importance of selectivity issue, no major promising solution has been presented in the previous studies. Many of the previous research works present a very case specific solution. Changing reaction conditions, such as temperature, pH, and solvent, was reported to help selective decomposition of certain chemicals (Lu et al., 2015; Bae et al., 2013; Yamamoto et al., 2013; Almquist and Biswas, 2001). Considering the heterogeneous nature of TiO_2 photocatalysis, i.e., adsorption followed by oxidation, many attempts have been given to physicochemical modifications of TiO_2 materials to facilitate selective access of target chemicals to the modified TiO_2 surface. These include doping of TiO_2 with other elements and imprinting of TiO_2 with molecular recognition sites (Xu et al., 2014; Inumaru et al., 2004; Ghosh-Mukerji et al., 2001). In most cases a secondary material introduced to TiO_2 is required to demonstrate unique chemical affinity for one specific target chemical. The approach with ultimate selectivity is hard to apply to treatment of a mixture of various target chemicals in the presence of NOM.

1.4. Proposed Idea and Hypothesis

Considering NOM is comprised of large macro-molecules (Ghosh and Schnitzer, 1980) while target chemicals (e.g., pharmaceuticals) are typically small micro-molecules, prevention of large size NOM from accessing the TiO_2 surface can potentially enhance decomposition of various small targets. Previously, the concept of such size exclusion has been implemented by introducing a secondary material with a controlled porous structure to TiO_2 such as a porous shell of silica and a silica sheet of

clay (Ide et al., 2011; Yoneyama et al., 1989). Molecules larger than the porous structure surrounding TiO_2 particles cannot access the TiO_2 surface and thus they are decomposed much less than small molecules accessible to the TiO_2 surface. The simple size exclusion seems attractive. However, synthesis of such a hybrid material is practically not easy and the size exclusion approach commonly requires a secondary material. In particular, introduction of a secondary material to increase selectivity usually accompanies low reactivity due to reduced active sites, low light utilization, and slow mass transfer (Yoneyama et al., 1989). In order to solve the common problem with the size exclusion approaches, we recently communicated a simple idea that even pure TiO_2 engineered with a porous structure has a high potential for the size exclusion (Zakersalehi et al., 2013). As depicted in Figure 1.2., Target molecules smaller than the pore size access the internal surface of TiO_2 while NOM larger than the pore size stays only at the external surface of TiO_2 (i.e., grain boundary).
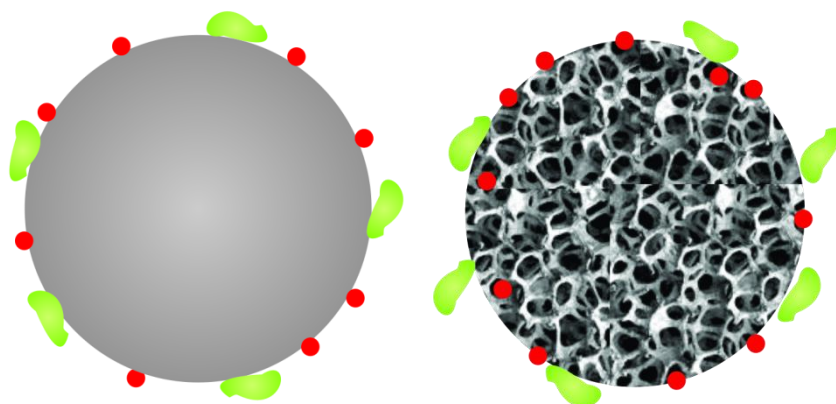
Figure 1.2. Photocatalytic decomposition of target contaminant in competition with NOM. I) Concurrent decomposition of NOM onto nonporous TiO_2 and lower decomposition rate of target contaminant. II). Due to smaller size of target contaminants, the internal surface of porous TiO_2 is accessible while large size NOM is suppressed on grain boundary.

Enhanced decomposition of small targets is also possible because the catalytic surface area is originated predominantly by internal surface. After the pioneering work, we have further investigated detailed mechanism on the size exclusion onto porous TiO_2. In this present study, we synthesized and tested a series of TiO_2 materials with optimum porous structures for the given conditions, and examined decomposition of ibuprofen (IBP, a pharmaceutical), Methylene blue (MB, a well-studied synthetic dye)

and Microcystin-LR (MC-LR, a biological toxin) as target chemicals with different sizes in the presence of Humic Acid (HA) as competing model NOM. It is focused how a specific TiO_2 porous structure, of which size is between sizes of a target and NOM, affects size exclusion of NOM and mass transfer of a target. We hypothesized that selecting a proper pore size has a tradeoff impact on selectivity and reactivity, e.g., pore size much smaller than NOM and slightly larger than a target is beneficial to selectivity due to better exclusion of NOM, but adverse to reactivity due to slow mass transfer of even the target. We have validated this approach we by changing the molecular size of target contaminants within the range of 1-3 nm while maintaining other parameters such as type and size of NOM. The correlation between pore-size distribution of TiO_2 and their selectivity behavior was explained. Also control experiments using non-porous TiO_2 were performed in parallel for the sake of comparison.

1.5. Goal and Objectives

The goal of this study is to pioneer novel physiochemical strategies for enhancing selectivity of TiO_2 photocatalysis toward target water contaminants in the presence of abundant non-toxic NOM.

1.5.1. Objective I: To verify and evaluate the presented size-exclusion hypothesis (Section 1.4.) that tailor-designing the porous structure of TiO_2 itself can contribute to physical retention of NOM, contributing to better selectivity. This phase of study includes: i) Synthesis of meso-porous TiO_2 with proper throat size, favorable for adsorption of target contaminants, ii) Verification of proposed method in terms of pure adsorption in dark condition, iii) Verification of proposed size-exclusion mechanism in regards to photocatalytic activity by employing various combinations of target/competing compounds.

Significance: This is a pioneering comprehensive study that proposes a general approach for enhancing preferential decomposition by use of pure TiO_2 material. Despite previously presented methods this approach does not require other complex physical and chemical modifications to TiO_2. In the previous studies, the size-exclusion mechanism was generally implemented by introduction of a secondary material to TiO_2. The secondary material was mainly composed of meso-porous SiO_2 material which is not chemically reactive. They secondary layer could also pose an adverse effect in terms of

mass transfer limitation of target contaminants. Also our proposed method gives us great flexibility in tailor designing the degree of porosity and size of throat simply by modifying sol-gel method.

1.5.2. Objective II: To increase preferential decomposition of anionic and cationic target contaminants by adjusting reaction conditions with focus on TiO_2 surface charge and in combination with proposed size-exclusion approach. We can utilize amphoteric properties of TiO_2 material to induce surface charge simply by changing reactor pH. The correlation Zeta potential of TiO_2 material will be measured over pH range and the results will be correlated with decomposition of anionic and cationic compounds. To verify proposed hypothesis, a series of anionic (IBP, SMX) and Cationic (MB) target contaminants will be used as target compounds and their ionization state will be correlated with their decomposition behavior.

Significance: The molecular shape, ionization state and consequently charge of compounds are largely dependent on pH value. On the other hand the surface charge of TiO_2 can be adjusted by changing medium pH. pH adjustment can be utilized as an effective factor to govern the photocatalytic reaction in the favor of target contaminants. It is also notable, due to porous structure of TiO_2, this method utilizes porous structure as well as surface charge to increase the preferential adsorption. Knowing that adsorption behavior of competing NOM in different pH is generally similar to anionic target contaminants, one cannot achieve great selectivity only by means of pH adjustment. As an alternative in this study we proposed a mesoporous structure to retain large NOM while favorable pH can increase the adsorption followed by decomposition of target compounds. We have also demonstrated the synergic effect of both methods is larger in terms of selectivity by performing control experiments using non-porous TiO_2 nanoparticles.

1.6. References

Almquist, C. B.; Biswas, P. (2001) The Photo-oxidation of Cyclohexane on Titanium Dioxide: an Investigation of Competitive Adsorption and its Effects on Product Formation and Selectivity. *Appl. Catal. A: Gen.*, 214, 259−271.

Autin, O.; Hart, J.; Jarvis, P.; MacAdam, J.; Parsons, S. A.; Jefferson, B. (2012) Comparison of UV/H_2O_2 and UV/TiO_2 for the Degradation of Metaldehyde: Kinetics and the Impact of Background Organics. *Water Research*, 46, 5655−5662.

Bae, S.; Jung, J.; Lee, W. (2013) The Effect of pH and Zwitterionic Buffers on Catalytic Nitrate Reduction by TiO_2-supported Bimetallic Catalyst. *Chem. Eng. J.,* 232, 327−337.

Deng, Y.; Zhao, R. (2015) Advanced Oxidation Processes (AOPs) in Wastewater Treatment. *R. Curr Pollution Rep*, 3, 167−176.

Ghosh, K.; Schnitzer, M. (1980) Macromolecular Structures of Humic Substances. *Soil Science.* 129, 266−276.

Ghosh-Mukerji, S.; Haick, H.; Schvartzman, M.; Paz, Y. (2001) Selective Photocatalysis by Means of Molecular Recognition. *J. Am. Chem. Soc.,* 123, 10776−10777.

Ide, Y.; Koike, Y.; Ogawa, M. (2011) Molecular Selective Photocatalysis by TiO_2/nanoporous Silica Core/Shell Particulates. *J. Colloid Interface Sci.,* 358, 245−251.

Inumaru, K.; Murashima, M.; Kasahara, T.; Yamanaka, S. (2004) Enhanced Photocatalytic Decomposition of 4-nonylphenol by Surface-organografted TiO_2: a Combination of Molecular Selective Adsorption and Photocatalysis. *Appl. Catal. B: Environ.,* 52, 275−280.

Kavurmaci, S. S.; Bekbolet, M. (2014) Non-selective Oxidation of Humic acid in Heterogeneous Aqueous Systems: a Comparative Investigation on the Effect of Clay Minerals. *Environ. Technol.* 35, 2389−2400.

Lazar, M. A.; Daoud, W. A. (2013) Achieving Selectivity in TiO_2-based Photocatalysis. *RSC Adv.*, 3, 4130−4140.

Lu, X.; Song, C.; Jia, S.; Tong, Z.; Tang, X.; Teng, Y. (2015) Low-temperature Selective Catalytic Reduction of NOX with NH_3over Cerium and Manganese Oxides Supported on TiO_2–Graphene. *Chem. Eng. J.,* 260, 776–784.

Maruya, K. A.; Dodder, N. G.; Sengupta, A.; Smith, D. J.; Lyons, J. M.; Heil, A. T.; Drewes, J. E. (2016) Multimedia screening of contaminants of emerging concern (CECS) in coastal urban watersheds in southern California (USA). *Environmental Chemistry*, 8, 1986-1994.

Matilainena, A.; Vepsäläinenc, M.; Sillanpää, M. (2010) Natural organic matter removal by coagulation during drinking water treatment: A review. Advances in Colloid and Interface Science, 159, 189–197.

Park, H.; Kim, H.; Moon, G.; Choi, W. (2016) Photoinduced charge transfer processes in solar photocatalysis based on modified TiO2. Energy Environ. Sci., 9, 411-433.

Paz, Y. (2006) Preferential Photodegradation-Why and How?. *C.R. Chimie,* 9, 774−787.

Rasoulifard, M.; Fazli, M.; Eskandarian, M. (2014) Degradation of Organophosphorus Pesticide Diazinon Using Activated Persulfate: Optimization of Operational Parameters and Comparative Study by Taguchi's Method. *J. Ind. Eng. Chem.,* 20, 3695−3702.

Richardson, S. D.; Ternes, T. A. (2014) Water Analysis: Emerging Contaminants and Current Issues. *Anal. Chem.,* 86, 2813−2848.

Volk, C.; Wood, L.; Johnson, B.; Robinson, J.; Zhuc, H. W.; Kapland, L. (2002) Monitoring Dissolved Organic Carbon in Surface and Drinking Waters. *J. Environ. Monit.,* 4, 43−47.

Xu, S.; Lu, H.; Chen, L.; Wang, X. (2014) Molecularly Imprinted TiO_2 Hybridized Magnetic Fe_3O_4 Nanoparticles for Selective Photocatalytic Degradation and Removal of Estrone. *RSC Adv.*, 4, 45266−45274.

Yamamoto, A.; Mizuno, Y.; Teramura, K.; Shishido, T.; Tanaka, T. (2013) Effects of Reaction Temperature on the Photocatalytic Activity of Photo-SCR of NO with NH_3 Over a TiO_2 photocatalyst. *Catal. Sci. Technol.*, 3, 1771−1775.

Yoneyama, H.; Haga, S.; Yamanaka, S. (1989) Photocatalytic Activities of Microcrystalline TiO_2 Incorporated in Sheet Silicates of Clay. *J. Phys. Chem.*, 93, 4833−4837.

Zakersalehi, A.; Nadagouda, M.; Choi, H. (2013) Suppressing NOM Access to Controlled Porous TiO_2 Particles Enhances the Decomposition of Target Water Contaminants. *Catal. Comm,* 41, 79−82.

CHAPTER 2

Study on Size Exclusion of NOM onto Porous TiO$_2$ for Preferential Target Contaminants Decomposition

In this chapter we have examined a purely physical approach in to achieve preferential decomposition. In order to minimize the adverse effect of NOM, we have investigated physical size exclusion of large natural organic matter onto mesoporous TiO$_2$ photocatalysts, which allows small target contaminants to freely access the porous structure for following chemical reaction. The size-exclusion was implemented by utilizing a precisely designed meso-porous structure of TiO$_2$ photocatalysts. Various treatment scenarios tested with different targets (Ibuprofen, Microcystin-LR, Methylene blue) and competitors (Humic acid) and a set of mesoporous TiO$_2$ materials proved the size exclusion mechanism can differentiate organic compounds simply based on their size difference. Porous TiO$_2$ also demonstrated more reactivity in terms of TOC removal which is favorable. Discussion was made on the impact of the porous structure of TiO$_2$ on selectivity and reactivity, considering size difference among targets < TiO$_2$ pores < competitors as well as mass transfer limitation of even a target to small pores. It was discovered along with increase in size of model NOM while maintaining the size of target contaminant better selectivity was achieved on porous TiO$_2$. Also the role of inter-pore adsorption showed to be the highest in cases the reactive surface area was a limiting factor. Discussion was made on optimum porous structure for decomposition of IBP. Despite larger surface area provided in case of extremely porous TiO$_2$ material, the selectivity showed to decline compared to TiO$_2$ material with moderate porosity. The loss of selectivity was correlated with formation larger throat size in case of extreme porosity which cannot effectively exclude the competing HA from entering the pores. Sensitivity analysis showed this approach is most effective in cases concentration of target contaminant is relatively high compared to competing NOM.

2.1. Introduction

2.1.1. Synthesis of Meso-porous TiO$_2$ with Narrow Pore Size Distribution

TiO$_2$ photocatalysts were synthesized by following a sol-gel process employing Titanium (IV) isopropoxide (TTIP) as a precursor material. In particular, Tween 80 surfactant, which is known to form a self-assembled structure, was used as a pore template in the sol-gel method to fabricate mesoporous TiO$_2$ materials. Porous TiO$_2$ (P-TiO$_2$) particles were fabricated from an organic/inorganic sol composed of Tween 80, iPrOH, acetic acid, and TTIP at a molar ratio of R:45:6:1. For sol preparation, proper amount of Tween 80, (R=0 for control particles and R=1,2,4 for porous TiO$_2$) were dissolved in iPrOH. For porous TiO$_2$ (P-TiO$_2$) the optimum amount of Tween 80 was selected through a set of preliminary experiments. The formation of TiO$_2$ using TTIP as precursor is generally initiated with addition of water. To generate water in situ via the esterification reaction with iPrOH, acetic acid was added into the solution. A TiO$_2$ inorganic network was forms around the self-assembled surfactant molecules after hydrolysis of the added TTIP with the in situ generated water. After drying the gel at room temperature to remove solvents, it was calcined to pyrolyze the surfactant assembly and to transform the crystal phase of TiO$_2$, leaving a porous structure in an anatase TiO$_2$ inorganic network. Calcination temperature was increased at a ramp rate of 3 °C min^{-1} and it was held at 500 °C for 1 hr. and cooled down naturally. A series of TiO$_2$ materials were denoted as C-TiO$_2$ for control (nonporous, R=0) TiO$_2$ and P-TiO$_2$ (porous, R=2) TiO$_2$. Effect of porous structure on selectivity was later studied using P$_1$ and P$_4$.

To determine the structural properties of the synthesized TiO$_2$ particles such as surface area, porosity, and pore size distribution, which are directly associated with results on selectivity and reactivity later, they were characterized with a porosimetry analyzer (Tristar 3000, Micromeritics).

TiO$_2$ particles were visually inspected by using a high-resolution transmission electron microscope (HR-TEM, JEOL JEM-2010F). The X-ray diffraction pattern of TiO$_2$ particles was investigated on a Kristalloflex D500 diffractometer (Siemens) to determine their crystal structure including crystal phase and size.

2.2. Reagents and material selection

2.2.1. Ibuprofen: 2-[4-(2-methylpropyl) phenyl] propanoic acid is a common nonsteroidal anti-inflammatory drug widely used in the treatment of pain and fever and It is considered as one of the frequently detected PPCPs compounds (Wen et al. 2014). Incompletely absorbed medication is released into the sewage system along with unused drugs that may be disposed via municipal drains. Other potential sources to the environment include leachate from landfill sites and wastewater discharges from hospital wastes and industrial manufacturing. Ibuprofen's physiochemical properties (i.e. water solubility, low volatility) suggest a high mobility in the aquatic environment, and consequently, it is a commonly detected in water resources. Although the effects on humans from low-level drinking water contamination by PPCPs are not currently fully understood, growing concern on the occurrence, fate, and possible effects of such substances in the environment. The molecular structure of IBP have been depicted in Figure 2.1.. It is a relatively small molecule with molecular weight of 206 g mol^{-1}, and the hydrodynamic molecular size of IBP was measured by Zeta sizer (Horiba, SZ-100) to be 1.0 nm in aqueous solution.
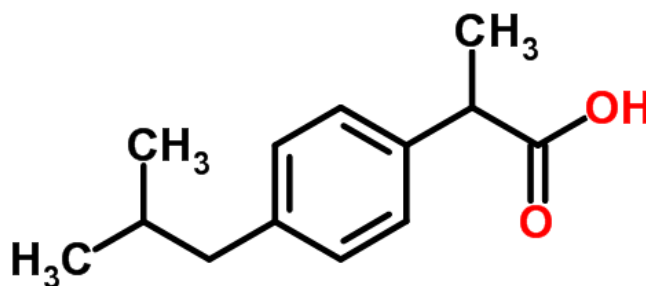
Figure 2.1. Molecular Structure of IBP $C_{13}H_{18}O_2$

2.2.2. Methylene Blue: methylthioninium chloride is a widely studied dye. It has several applications as pharmaceutical, industrial dye, pH indicator and a model contaminant in the field of water treatment. Its molecular formula is $C_{16}H_{18}ClN_3S$ with molecular weight of 319.85 g.mol^{-1} and with average hydrated molecular length around 1.8 nm. The molecular structure of MB have been shown in Figure 2.2..
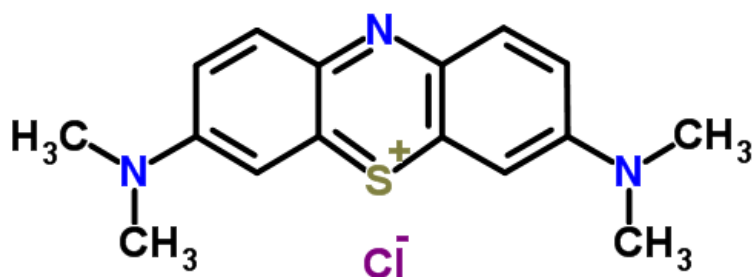
Figure 2.2. Molecular Structure of MB $C_{16}H_{18}CIN_3S$

2.2.3. Microcystin-LR: Microcystins are reported to be the most commonly occurring cyanotoxins found in water. The most commonly detected microcystin is microcystin-LR which has been reported to have chronic and acute toxicity. Acute exposure can results in hepatic injury and in extreme cases this can be deadly (Dunn, 1996). Also tumour-promoting characteristics of MC-LR can lead to serious health problems such as primary liver cancer through prolong exposure to low concentrations of MC-LR (Yu, 1994). In this regard a worldwide effort has been focusing on treatment of contaminated water. It have been established that most conventional water treatment systems, suffer from effective removal of MC-LR (Keijola et al., 1988; Lahti and Hiisvirta, 1989; Lawton and Robertson, 1999). For instance chlorination of MC-LR during disinfection process can result in generation of disinfection byproducts such as monochloro-microcystin, monochloro-dihydroxy-microcystin, dichloro-dihydroxy-microcystin and trichloro-hydroxy-microcystin which can be harmful active ingredients (Merel et al. 2009). In this study we have used MC-LR since it is contaminants of concern and also due to its size distribution. The molecular structure of MC-LR has been shown in Figure 2.3. The hydrodynamic length of MC-LR was measured to be approximately 3nm.
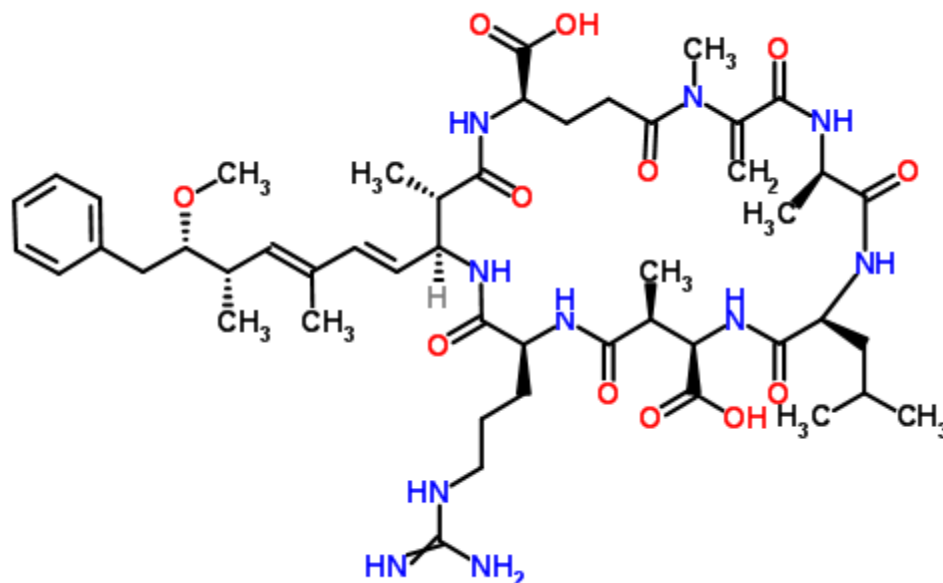
Figure 2.3. Molecular Structure of MC-LR $C_{49}H_{74}N_{10}O_{12}$

The MC-LR used in this experiment was purchased from Cayman Chemical in methanol solution form and it was dissolved in carbon free water.

2.2.4. Humic Acid: to illustrate the adverse effect of NOM, Humic acid was used in this experiment. They generally form the major portion of the dissolved organic matter in surface water that represents 90% of dissolved organic carbon (Corin et al. 1996). They are mainly formed during decay of plants and dead animals and they are mostly comprised of large macromolecules. The molecular structure of the HA used in this experiment is shown in Figure 2.4.. It should be noted that HA is comprised of a complex molecule and it shows a diverse size distribution in aqueous condition.
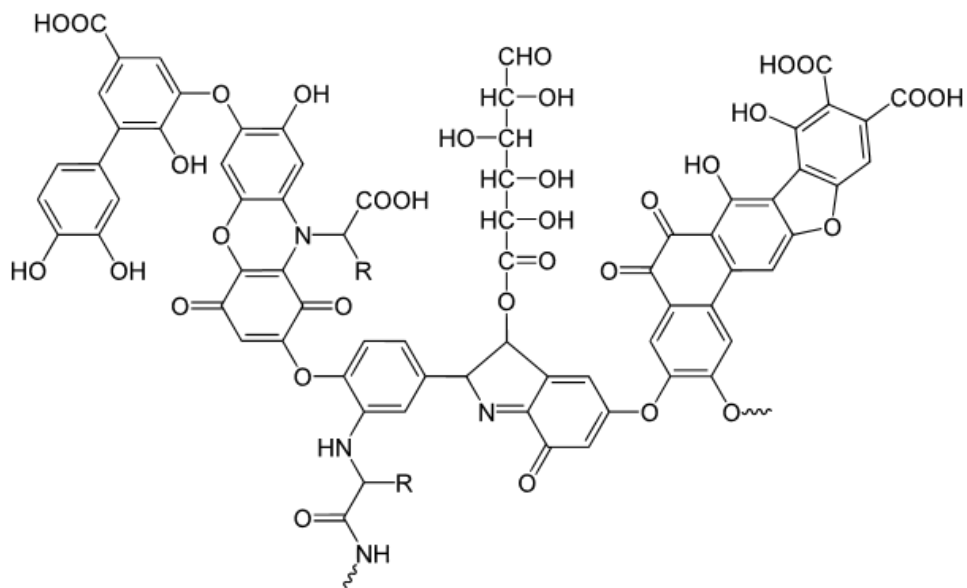
Figure 2.4. Molecular Structure of Humic Acid $C_{187}H_{186}O_{89}N_9S_1$

Compared to target contaminants we observed a considerably wider size distribution for source HA. In order to better understand the role of molecular size of species, HA was fractionated prior to experiment.

Classification of HA: To achieve a higher degree of uniformity, the HA was fractionated prior to experiment. The HA was classified into three size range using a ultrafiltration cell (Amicon Model-8200 series). An stock solution of HA with initial concentration of around 100 mg L^{-1} as TOC was filtered using 0.45 μm paper filter, the retained portion was re-suspended by carbon free water and used as large model NOM, denoted by HA_L in this study. The filtrate from previous step was used as feed for ultrafiltration cell equipped with regenerated cellulose membrane disc with nominal molecular weight cutoff of 100,000 g mol^{-1}. Transmembrane pressure was set to 0.5 atmosphere and he retained portion was then re-suspended in carbon free water and used as competing NOM throughout the experiment denoted by HA (or HA_M In cases different sizes of HA were used). The filtrate from ultrafiltration process was denoted as HA_S. The properties of compounds used in this study have been presented in Table 2.1.

Table 2.1 Information on the molecular structure of chemicals tested for size exclusion in this study.

Chemical	Ibuprofen	Methylene Blue	Microcysin-LR	Humic Acid
Acronym	IBP	MB	MC-LR	HA
Molecular formula	$C_{13}H_{18}O_2$	$C_{16}H_{18}ClN_3S$	$C_{49}H_{74}O_{12}N_{10}$	N/A
Molecular weight [g mol^{-1}]	206.3	319.85	995.2	N/A
Equivalent size [nm]	~1.0	~1.8	~3.0	Variable (3.3-17.0 nm average)
Role in this study	Target	Target	Target	Competitor

The percentage of each size class was determined by measuring TOC in each filtrate since re-suspension of retained HA is not 100% effective. Table 2.2 lists the quantity and average equivalent size of each class:

Table 2.2 Size fraction and their TOC contribution

Nominal Class Size	Acronym	Percentage by TOC (%)	Avg. Equivalent size (nm)
>0.45 µm	HA$_{large}$	13	17.0
0.45µm> > 8 nm	HA$_M$	45	8.1
8 nm >	HA$_{small}$	42	3.8

The size measurement was carried out by dynamic light scattering technique. No pre-sonication was applied and measurement time was set to three rounds of 60 second runs at 20 ^{o}C without noise cancelation.

2.3. Photocatalytic experiment

The photocatalytic reactivity of the synthesized TiO$_2$ particles was evaluated with using three set of target contaminants and competing HA as a model NOM. The degree of selectivity was measured by comparing performance of each set of TiO$_2$ particle in pure and competing conditions. The competing condition was comprised of introducing equal TOC concentrations of target contaminant and HA as model

NOM. To quantify selectivity, the IBP in the absence (no competition) and the presence (competition) of HA to determine the degree of their selectivity towards IBP. Concentrations of IBP and HA were the same at each 10 mg L^{-1} as TOC. (Concentration of HA was defined here with total organic carbon (TOC) and thus its actual concentration was at 17.9 mg L^{-1}, considering HA has around 56% carbon content). The decomposition experiment was conducted at pH=6.5 with buffer solution in order to prevent substantial change in reactor. It is known the pH can greatly affect the adsorption as well as the kinetics of reaction and subsequently it can change the surface charge of TiO_2. TiO_2 particles were initially dispersed by a sonicator (Cole-Parmer 8891). A borosilicate glass batch reactor containing the chemicals and TiO_2 suspension at 0.5 g L^{-1} under vigorous mixing was irradiated with two 15W low pressure mercury ultraviolet (UV) lamps emitting 365 nm. The same batch test was repeated with MB with 10 mg L^{-1} as TOC concentration. In the batches containing MC-LR, the TOC concentration was set to 5 mg L^{-1} due to extreme toxicity. Dark condition adsorption was done in similar conditions without exposure to any light. In both cases samples were taken out every 15 minutes and filtered using a 0.22 µm membrane to filter out TiO_2 particles.

2.4. Chemical analysis

The molecular size distribution of the chemicals was examined on a dynamic light scattering size analyzer (Horiba SZ-100). Due to significant interfere from HA and TiO_2, the size distribution of each compound was measure in pure condition. Total Organic Carbon (TOC) concentration was monitored using a TOC analyzer (Shimadzu TOC-Vcsn). Concentration of IBP was monitored using a reversed-phase high performance liquid chromatography (Agilent 1200 series) equipped with a C-18 column (Agilent). For the detection of IBP, mobile phase was a mixture of phosphoric acid and acetonitrile (50:50% v/v) and a UV detector was set at 214 nm. Detection of MB was carried out by detection at 246 nm and mobile phase was comprised of 0.34% phosphoric acid (adjusted to pH 3.0 with triethylamine)-acetonitrile(77:23). For the detection of MC-LR, mobile phase was a mixture of 0.05% trifluoroacetic acid and acetonitrile (80:20% v/v) and peak was detected at 238 nm.

2.5. Results and discussions

2.5.1. Pore size and hypothesis

Ideally, the porous structure of TiO_2 should be accessible only by the target chemical for the successful size exclusion of a competing chemical. It is beneficial to have pore size of TiO_2 larger than a target chemical and smaller than a competing chemical (e.g., NOM). If pore size is smaller than a target and NOM, none of them can access the porous structure, resulting in no selectivity. On the other hand, if pore size is larger than a target and NOM, all of them access the porous structure, also resulting in no selectivity. As a result, pore size should be between sizes of a target and NOM if possible. Pore size can affect selectivity based on size exclusion of NOM as well as reactivity based on mass transfer of a target in an opposite way, i.e., tradeoff effect. As pose size goes down close to size of a target, more significant size exclusion of NOM occurs while slow mass transfer of even a target to the small pores occurs simultaneously. Selectivity can be maximized but overall reactivity even towards a target might be decreased. On the other hand, as pose size goes up close to size of NOM, less significant size exclusion of NOM occurs while fast mass transfer of a target to the large pores occurs. Selectivity can be minimized but overall reactivity towards a target might be increased. This tradeoff effect would determine the overall reactivity towards target chemicals.

As a result, it is important to examine the effect of pore size of TiO_2 on the decomposition of a target in the presence of NOM, with respect to balance between selectivity and reactivity.

Figure 2.5. shows HR-TEM images of $C-TiO_2$ for control TiO_2 and $P-TiO_2$. Compared to the control $C-TiO_2$ showing a less porous structure, $P-TiO_2$ showed a well-developed mesoporous structure particularly originated from interconnected intraparticle pores which are favorable for mass transfer of molecules. As shown in Figure 2.5, $P-TiO_2$ had a collapsed, spherical, bicontinuous structure with a highly interconnected network, inducing a high porosity. This porous network can provide great surface area as well as facilitated mass transfer of species in and outside the network. On the other hand, $C-TiO_2$ shows a rather bulky structure with very limited random pores which could be attributed to organic impurities in sol.
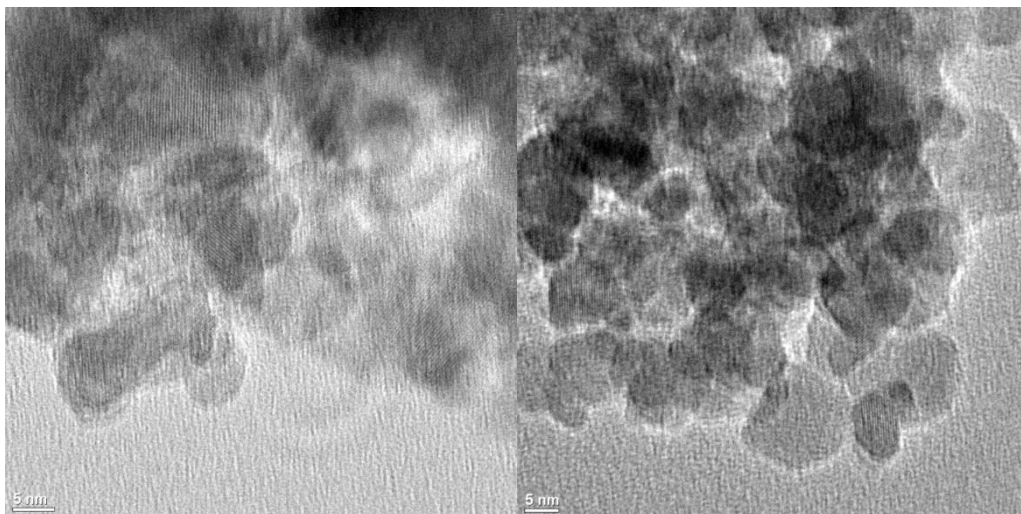
Figure 2.5. High-resolution transmission electron microscope of the a)- C-TiO$_2$ and b) P-TiO$_2$
Distinct hollow structure observed in P-TiO$_2$ could be attributed to free space originated from pyrolysis of organic surfactant during calcination process

The XRD pattern of TiO$_2$ is shown in Figure 2.6.. Both TiO$_2$ samples exhibited highly active anatase crystal phase. The crystal size at around 10 nm is known to be optimum for photocatalytic activity (Zhang *et al.*, 1998).
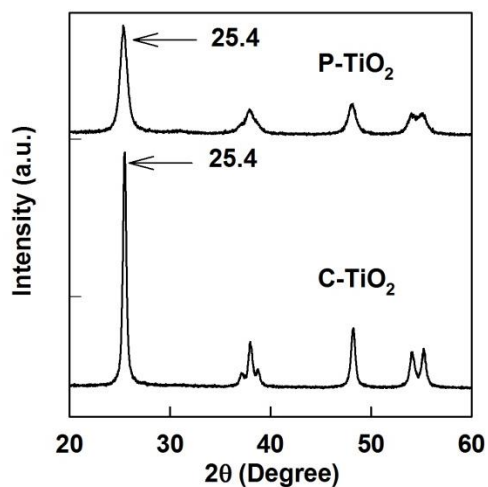
Figure 2.6. X-ray diffraction patterns of the P-TiO$_2$ and C-TiO$_2$

As shown in Figure 2.6., Both C-TiO$_2$ and P-TiO$_2$ reveal distinct response peak at 25.4° which corresponds to anatase crystalline phase (Nishanthia 2013). Response peak shows small decline in case

of P-TiO$_2$ which can be attributed to inhibiting effect of organic templates on crystal growth. This results evidences that both C-TiO$_2$ and P-TiO$_2$ are more or less similar in terms of crystalline characteristics. Physiochemical properties of C-TiO$_2$ and P-TiO$_2$ have been summarized in Table 2.3.

Table 2.3 Physiochemical properties of TiO$_2$ photocatalysts

Parameter	C-TiO$_2$	P-TiO$_2$
Surface area [m^2 g^{-1}]	13.7	76.4
Pore volume [cm^3 g^{-1}]	0.028	0.159
Porosity [%]	10.6	40.2
Pore diameter [nm]	7.38	7.31
Crystal phase	Anatase	Anatase
Crystal size	16.3	11.6
Porous nature	Control	Porous

2.5.2. Interaction of Molecular size and Porous Structure

Considering the heterogeneous nature of photocatalytic reactions and the short lifetime of hydroxyl radicals, the preferential adsorption of a target to the TiO$_2$ surface can result in its selective decomposition. Information on the molecular structure of the chemicals tested in this study is summarized in Figure 2.7. Size difference between a target chemical and a competing chemical should be significant enough to achieve size exclusion onto porous TiO$_2$ particles. It was hypothesized larger size difference induces better size exclusion. The decomposition kinetics of a target chemical should be less affected by the presence of NOM, which is a measure of selectivity in this study.
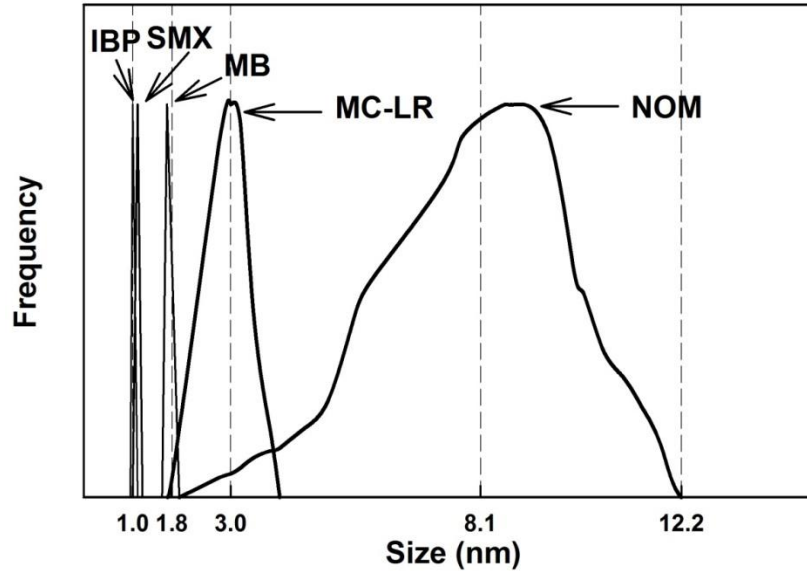
Figure 2.7. Size distribution Comparison of Target (IBP, SMX, MB, MC-LR) and competing HA.

As shown in Figure 2.7, the size distribution of IBP, MB and MC-LR show sharp peak at approximately 1 nm, 1.8 nm and 3 nm respectively. On the other hand model NOM demonstrated significantly wider size distribution. It should be noted some portions of NOM are in vicinity of 2-3 nm. The formation of secondary dynamic membrane during filtration could have separated some small portions of HA which appeared in re-suspended solution. Also complex nature of HA and its functional groups could have resulted in agglomeration of HA molecules to form larger macromolecules in range of 12 nm.

As shown in Figure 2.8. distinct porous structure is observed for the case of P-TiO$_2$ compared to C-TiO$_2$. The majority of pore volume is located within vicinity of 5-12 nm.
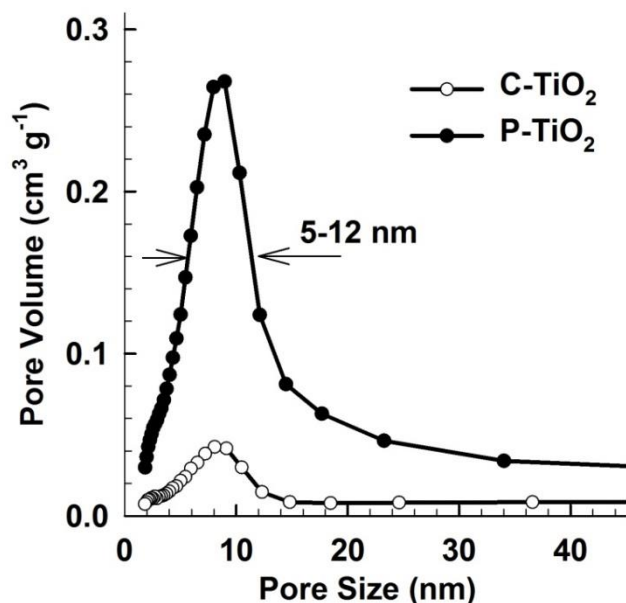
Figure 2.8. Pore size distribution of porous TiO_2 (P-TiO_2) vs. control TiO_2 (C-TiO_2). A relatively narrow

sharp peak in the range of 5-12 nm in case of P-TiO_2. This size distribution is believed to be large enough

to facilitate diffusion of target contaminants while small enough to suppress the physical access of model

NOM

The P-TiO_2 had a high specific area of 76.4 $m^2 g^{-1}$ and a high pore volume of 0.159 $cm^3 g^{-1}$

(porosity of 40.2%), compared to 13.7 $m^2 g^{-1}$ and 0.028 $cm^3 g^{-1}$ (porosity of 10.6%) for the C-TiO_2.

These results strongly support the significant role of the surfactant as pore directing agent for the

development of a porous inorganic network. It should be noted that only physical properties such as pore

size were differentiated while keeping other chemical properties same and thus any difference in target

decomposition rates in the following sections can be ascribed to the pore size difference.

2.5.3. Photocatalic Experiments

2.5.3.1. IBP decomposition in the presence of HA

Comparing decomposition kinetic of IBP under non-competitive condition without HA with that

under competitive condition with HA can explain the selectivity of TiO_2 photocatalysis. As shown in Figure

2.9. , control TiO_2 successfully decomposed IBP in the absence of HA. This is an ideal case that most of

researchers have set up to evaluate the reactivity of newly developed TiO_2 without considering real world complexity of treating an actual water matrix. However, in the presence of naturally abundant HA in water, IBP decomposition was significantly retarded from 100% to only 42% for 120 minutes of UV irradiation. This result well presents non-selective decomposition of IBP and HA since both molecules can freely access the surface of the control TiO_2 particles and they are decomposed, while competing each other.
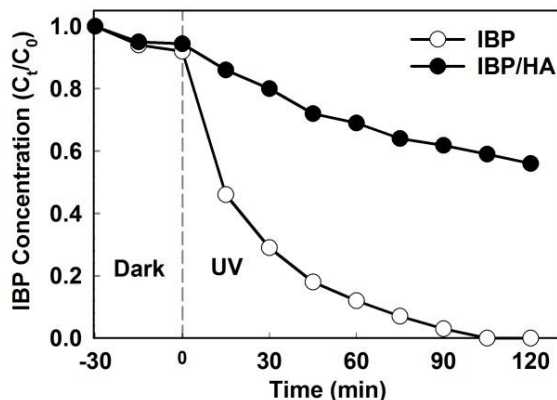
Figure 2.9. Decomposition of IBP onto C-TiO_2 in a non-competitive condition and in competition with HA

Figure 2.10 demonstrates decomposition of IBP onto P-TiO_2 particles. Compared to control experiment, P-TiO_2 showed significant reduction of IBP decomposition by presence of HA, i.e., the difference in IBP decomposition kinetics with HA and without HA was marginal.
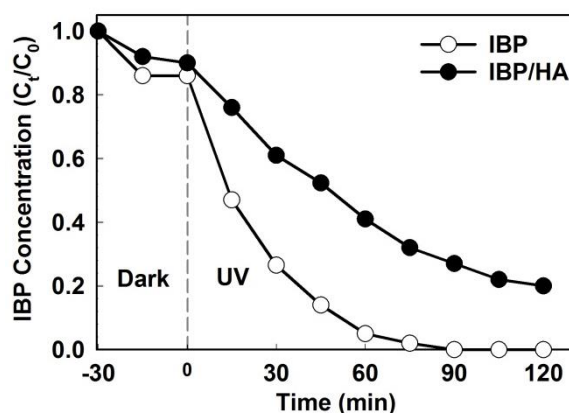
Figure 2.10 . Decomposition of IBP onto P-TiO_2 in a non-competitive condition and in competition with

HA

Dark condition adsorption of IBP in both cases (-30 min to 0 min) demonstrates the capacity of P-TiO$_2$ in terms of IBP adsorption. It should be noted that compared to C-TiO$_2$ the overall adsorption shows almost twice increase which supports the hypothesis of inter-pore adsorption of IBP. The adsorption equilibrium was achieved within 15 minutes in both cases. As shown in Figure 2.20 the decomposition reaction even in competing conditions follows pseudo first order regime which can support the hypothesis of minimal interaction of HA with TiO$_2$ surface.

2.5.3.2. MB decomposition in the presence of HA

Based on our hypothesis the selectivity achievement is purely a result of physical separation of patriating compounds. We used MB with slightly larger hydrodynamic molecular size (1.8nm compared to 1 nm in case of IBP) to validate this approach. Similarly the decomposition performance of C-TiO$_2$ is largely dependent on absence of HA. It was observed the decomposition of MB was reduced from complete removal to around 45% removal due to interaction with HA as shown in Figure 2.11.
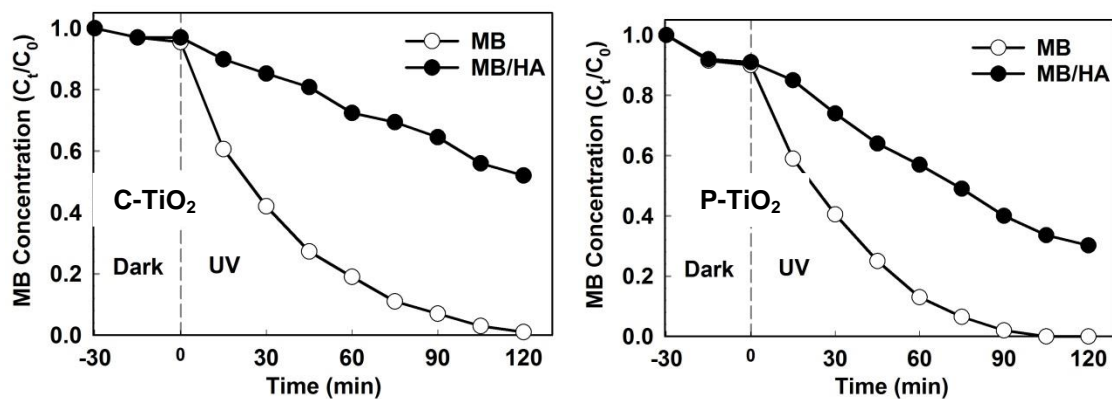
Figure 2.11. Photocatalytic decomposition of MB onto a) C-TiO$_2$ and b) P-TiO$_2$ in non-competitive condition and in competition with HA

It was observed that use of P-TiO$_2$ could recover the selectivity in some degree. In this case the decomposition reaction was declined from 100% to 61%. Lower selectivity of P-TiO$_2$ in this case could be attributed to larger size of MB which could result in mass transfer limitation for inter-pore adsorption as well as decomposition. It is also notable that presence of HA can affect the decomposition reaction not

only by scavenging the generated hydroxyl radicals but also it have been stablished that HA is capable of forming complex with organic compounds. Comparison between Figures 2.12. and 2.13. suggests the possible binding between MB and HA.
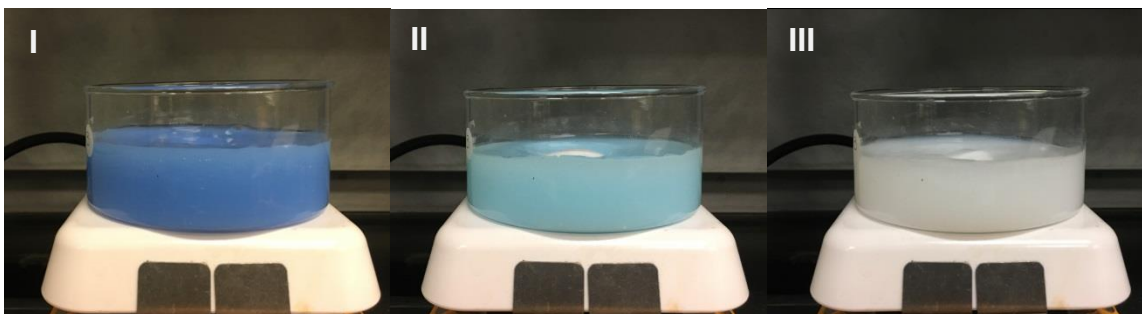
Figure 2.12. Photocatalytic decomposition of MB in pure condition, I) at t=0 minutes II) at t=30 minutes III) after 120 minutes of UV irradiation.

As shown in Figure 2.12. the de-colorizations of MB in pure condition suggesting complete primary decomposition of MB. On the other hand along with presence of HA, as shown in Figure 2.13. after 120 minutes of UV irradiation slight shade of dark blue can be observed in solution.
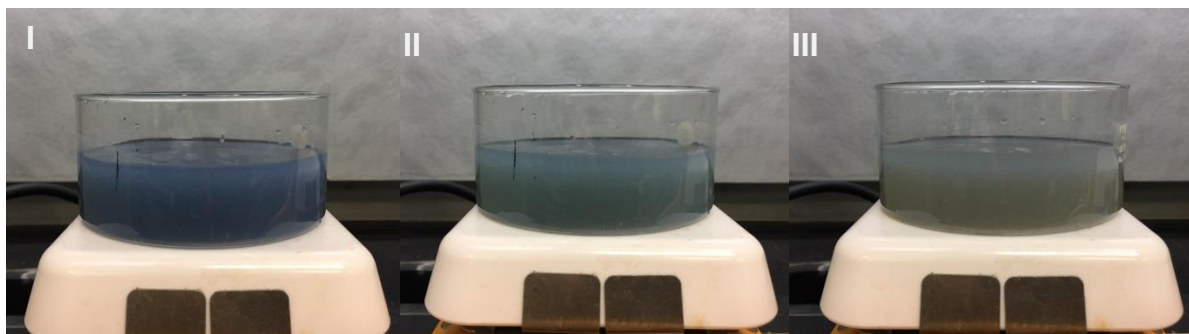
Figure 2.13. Photocatalytic decomposition of MB in competition with HA, I) at t=0 minutes II) at t=30 minutes III) after 120 minutes of UV irradiation.

It was notable the filtration of mixture with ultrafiltration cell with would result in removal of bluish color from solution suggesting that present MB in mainly is bonded to HA. This observation can be explained by charge characteristics of MB and HA at pH=6.5. From literature we know that MB at this pH is in cationic form while HA is in anionic form suggesting higher binding affinity for two compounds.

2.5.3.3. MC-LR decomposition in the presence of HA

Primary decomposition of MC-LR onto C-TiO_2 showed more or less similar retarding effect of model NOM on decomposition reaction. It should be noted that in almost all the cases we observed slightly less adsorption in both C-TiO_2 and P-TiO_2 once HA was introduced. This effect could be explained by the fact that some of the adsorption sites are occupied by competing NOM which is in agreement with our hypothesis. Similarly P-TiO_2 shows less sensitivity to presence of HA in terms of pure adsorption as well as photocatalytic decomposition. As shown in Figure 2.14., the primary decomposition of MC-LR in this case was achieved in a relatively shorter time for both cases.
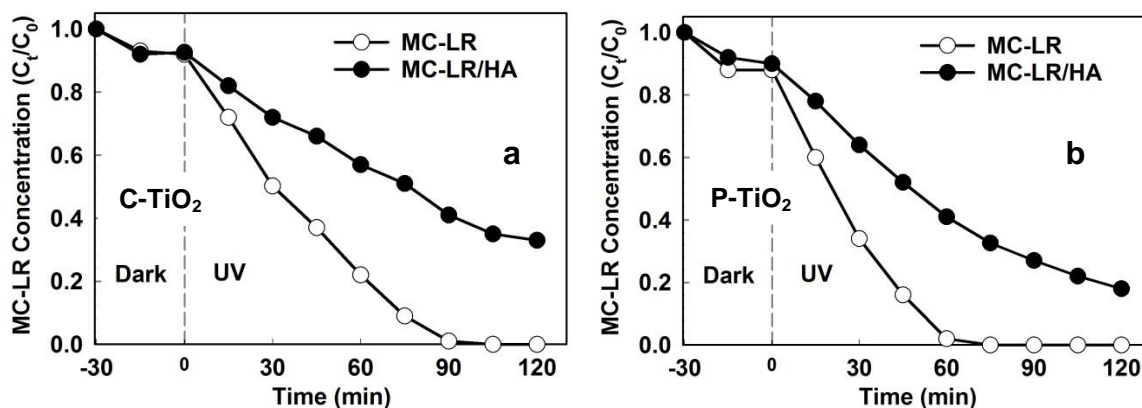
Figure 2.14. Photocatalytic decomposition of MC-LR onto a) C-TiO_2 and b) P-TiO_2 in non-competitive condition and in competition with HA

Lower initial concentration of MC-LR resulted in faster complete decomposition of MC-LR as expected. Overall the trend of selectivity in regards to size of target compound while the maintaining the size of competing NOM, demonstrates that smaller target compounds could be more selectivity decomposed onto P-TiO_2 evidencing the role of inter-pore active sites in decomposition reaction. We

28

believe the partial utilization of porous structure as well as adsorption of competing HA onto grain boundary could be the reason for partial selectivity. Also as demonstrated in experimental setup section, the presence of HA showed to significantly lower the light penetration into reactor, i.e. less OH generation.

2.5.4. Pores size distribution and selectivity

Ideally, the porous structure of TiO_2 should be accessed only by a target chemical for the successful size exclusion of a competing chemical. It is beneficial to have pore size of TiO_2 larger than a target chemical and smaller than a competing chemical (e.g., NOM). If pore size is smaller than a target and NOM, none of them can access the porous structure, resulting in no selectivity. On the other hand, if pore size is larger than a target and NOM, all of them access the porous structure, also resulting in no selectivity. In either case, the presence of NOM can significantly inhibit the decomposition of a target. As a result, pore size should be between sizes of a target and NOM if possible. Pore size can affect selectivity based on size exclusion of NOM as well as reactivity based on mass transfer of a target in an opposite way, i.e., tradeoff effect. As pose size goes down close to size of a target, more significant size exclusion of NOM occurs while more mass transfer limitation of even a target to small pores occurs simultaneously. Selectivity can be maximized but overall reactivity even towards a target might be decreased. On the other hand, as pose size goes up close to size of NOM, less significant size exclusion of NOM occurs while faster mass transfer of a target occurs.

As a result, it is important to examine the effect of pore size of TiO_2 on the decomposition of a target in the presence of NOM, with respect to balance between selectivity and reactivity. In addition to P-TiO_2 (with molar concentration of R=2) two meso-porous set of particles were synthesized using Tween 80 as a pore template. To demonstrate the effect of porous structure, IBP with the best selectivity result was selected . Decomposition of IBP in the presence of HA using C-TiO_2, P_1-TiO_2, P_2-TiO_2 and P_4-TiO_2 have been shown in Figure 2.15. In agreement with hypothesis along with incorporation of inter-pore adsorption sites in P_1-TiO_2, some selectivity enhancement was observed as shown in Figure 2.15 (b).
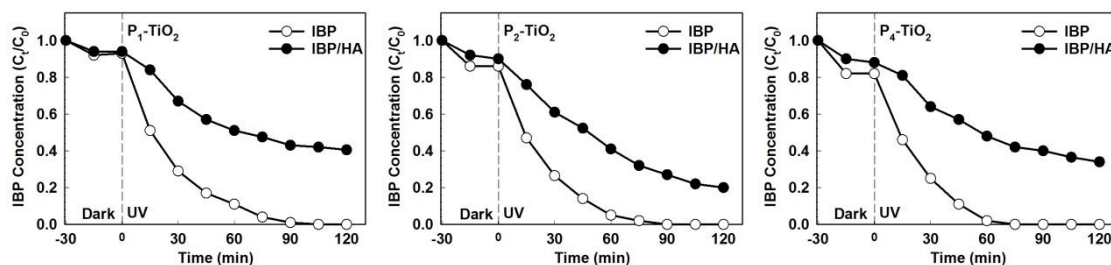
Figure 2.15. Effect of meso-porous structure of TiO_2 on photocatalytic decomposition of IBP. Greater selectivity along with increase in porosity from P_1-TiO_2 to P_2-TiO_2 and loss of selectivity due to defect structure and formation of unfavorably large throat size in P_4-TiO_2.

The overall trend in selectivity demonstrated that increasing porosity reaches an optimal point (P_2-TiO_2 in this case). Lower selectivity of P_1-TiO_2 compared to P_2-TiO_2 could be explained my mechanism stated earlier. Extremely low pore size distribution might be beneficial in terms of pure exclusion of HA. However an efficient photocatalytic decomposition requires effective mass transfer of target contaminants within th pores. Also reduced inter-pore surface area implies a relatively larger portion of photocatalytic reaction takes place at grain boundary which is accessible for HA. Increasing porosity to an extremely large amount showed to be ineffective rather weakening in terms of reactivity, despite larger surface area provided in P_4-TiO_2 compared to P_2-TiO_2. This effect can be explained by crystalline inhibition properties of pore directing agent. Also as predicted by size-exclusion model, extremely larger pores can impose an adverse effect since they are not capable of effective retention of large NOM on the outer surface of particle. In summary, increasing porosity showed to be beneficial to some point, after that regardless of higher provided surface area, selectivity showed to decline.

2.5.5. Impact of TiO_2 concentration on selectivity

To obtain additional insight into the competitive decomposition, the impact of catalysts concentration was studied herein. If the internal adsorption sites are efficient, the relative selectivity enhancement should show better results in cases where the surface area is a limiting factor. The TiO_2 concentration was changed in the range of 0.1 g L^{-1} to 1.0 g L^{-1} for the photocatalytic reactions using IBP with the best selectivity results. As shown in Figure 2.16., overall photocatalytic decomposition of IBP in

pure condition using 0.1 g L^{-1} demonstrated significant drop compared to the control concentration (0.5 g L^{-1}).
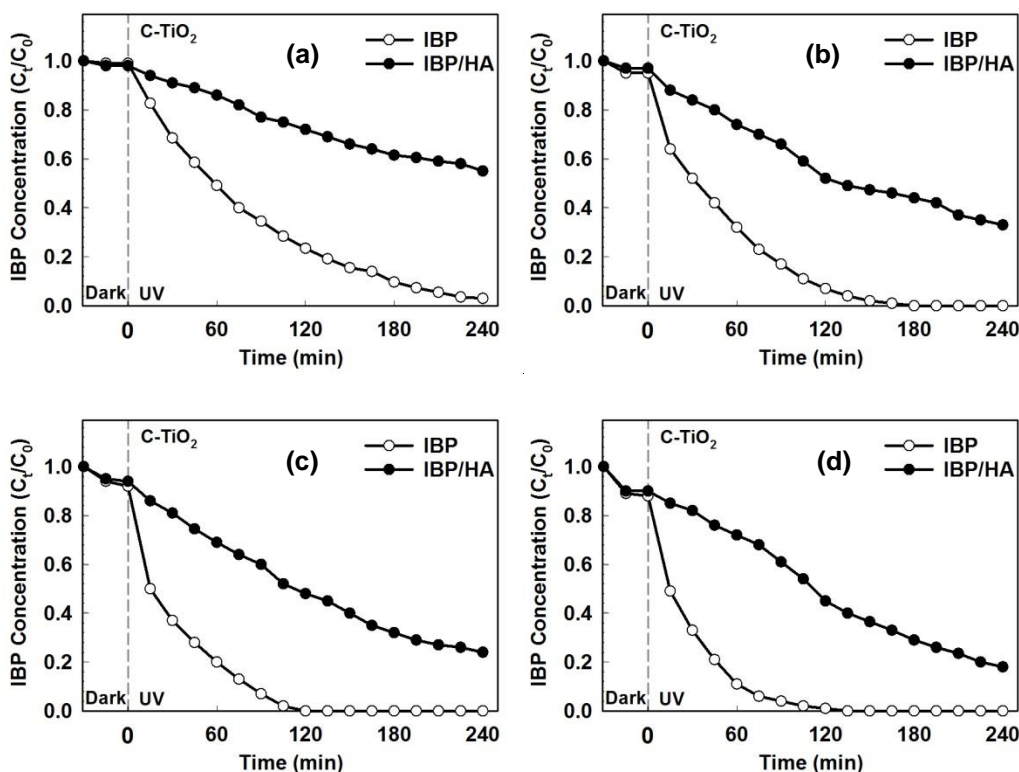
Figure 2.16. Photocatalytic decomposition of IBP onto C-TiO$_2$ a) using 0.1 g L^{-1} b) 0.25 g L^{-1} c) 0.5 g L^{-1} d) 1.0 g L^{-1}

It is notable the reactivity showed to be higher in case of P$_2$-TiO$_2$. Larger surface area provided by P$_2$-TiO$_2$ could have results in higher UV utilization and higher decomposition rate due to interpose decomposition. These results suggest the reactive surface area is a limiting factor in this case compared to control concentration experiment with extremely high concentration of TiO$_2$. Introduction of HA showed to have greater impact on decomposition using C-TiO$_2$ exhibiting even larger competition due to surface adsorption of HA which occupy the adsorption sites for IBP adsorption. On the other hand P-TiO$_2$ revealed significantly less sensitivity to introduction of HA. Comparison between C-TiO$_2$ and P-TiO$_2$ with 0.1 g L^{-1} concentration suggests that higher selectivity was achieved compared to case with 0.5 g L^{-1} concentration. Increasing in TiO$_2$ concentration from 0.1 g L^{-1} to 0.25 g L^{-1} demonstrated large increase in decomposition rate of pure IBP as shown in Figure 2.16 and Figure 2.17.
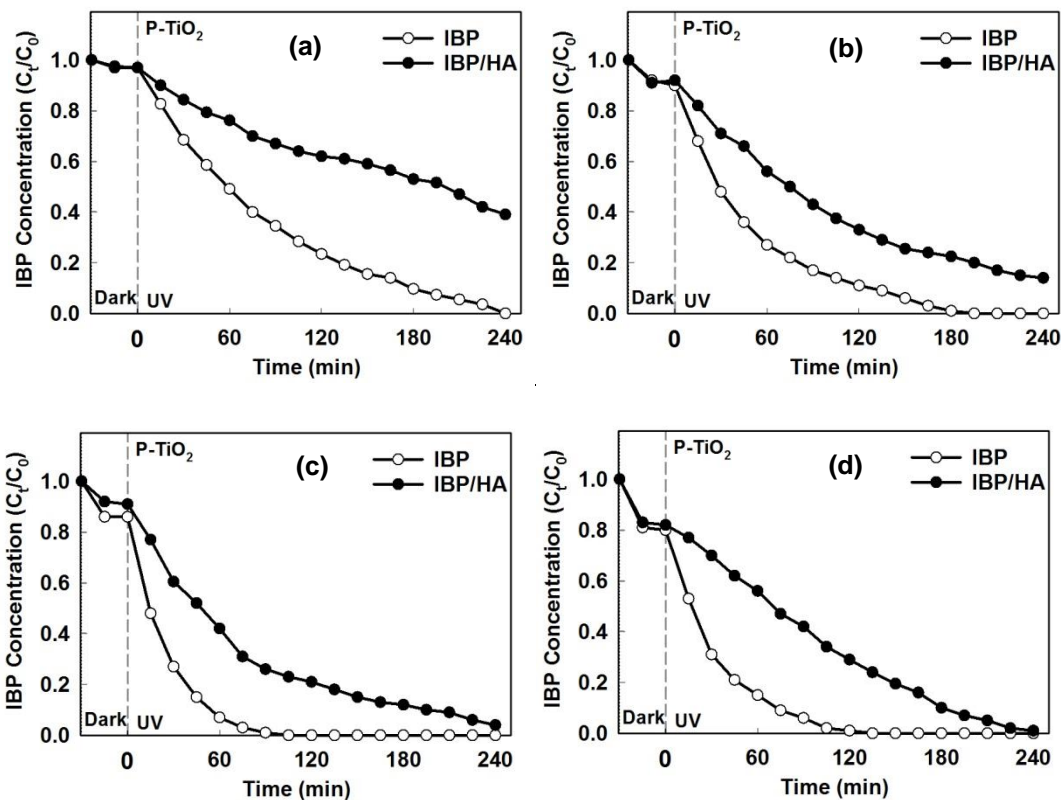
Figure 2.17. Photocatalytic decomposition of IBP onto P-TiO$_2$ a) using 0.1 g L^{-1} b) 0.25 g L^{-1} c) 0.5 g L^{-1} d) 1.0 g L^{-1}

In harmony with hypothesis, the decomposition rate of IBP is more sensitive to introduction of HA compared to 0.5 g L^{-1} case. Increasing TiO$_2$ concentration to 1 g L^{-1} showed to largely affect the initial adsorption of species as shown in Figure 2.17. The extremely large provided surface area in both C-TiO$_2$ and P-TiO$_2$ can explain this behavior. Despite large surface area provided, the decomposition kinetic showed decline compared to case with 0.5 g L^{-1}. The impact of TiO$_2$ concentration of pure decomposition of IBP have been shown in Figure 2.18. Generally larger concentration of TiO$_2$ resulted in greater concentration drop in dark conditions due to higher adsorption capacity of catalyst. Interestingly increasing TiO$_2$ concentration beyond 0.5 g L^{-1} showed to adversely affect the decomposition kinetics.

This effect can be attributed to light blockage due to low transparency of TiO_2 solution with 1 g L^{-1} concentration as pictured in Figure 2.18.
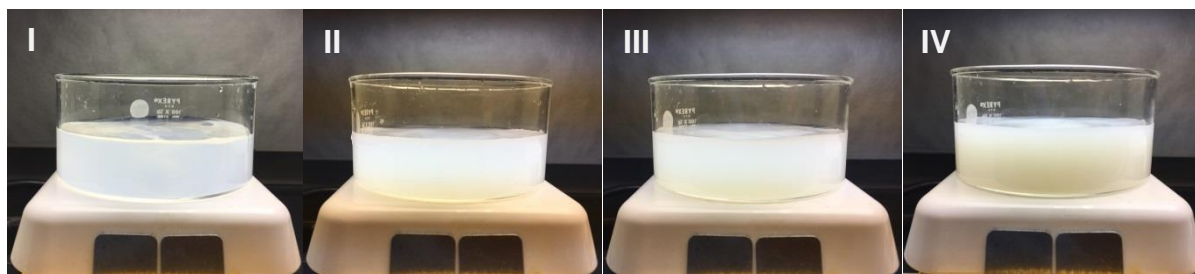
Figure 2.18. Decomposition of IBP in presence of P-TiO_2 I) 0.1 g L^{-1}, II) 0.2g g L^{-1}, III) 0.5 g L^{-1}, IV) 1.0 g L^{-1}. Lower UV light utilization due to lower transparency of suspension at high TiO_2 concentration.

2.5.6. Discussion of size distribution of model NOM

As shown in Figure 2.9. to Figure 2.14., along with decrease in size of target compound, higher size exclusion and consequently higher selectivity was achieved while maintaining the size of HA. The applicability of this method is largely dependent on size distribution of competing HA. To confirm the selectivity enhancement was purely a result of size exclusion we repeated the same experiments with different size distributions of HA. The HA was separated into three fractions as explained in section 2.2. The majority of HA falls within size distribution smaller than 0.45 µm. Photocatalytic decomposition of IBP in the presence of various fractions of HA have been presented in Figures 2.19 through Figure 2.20.
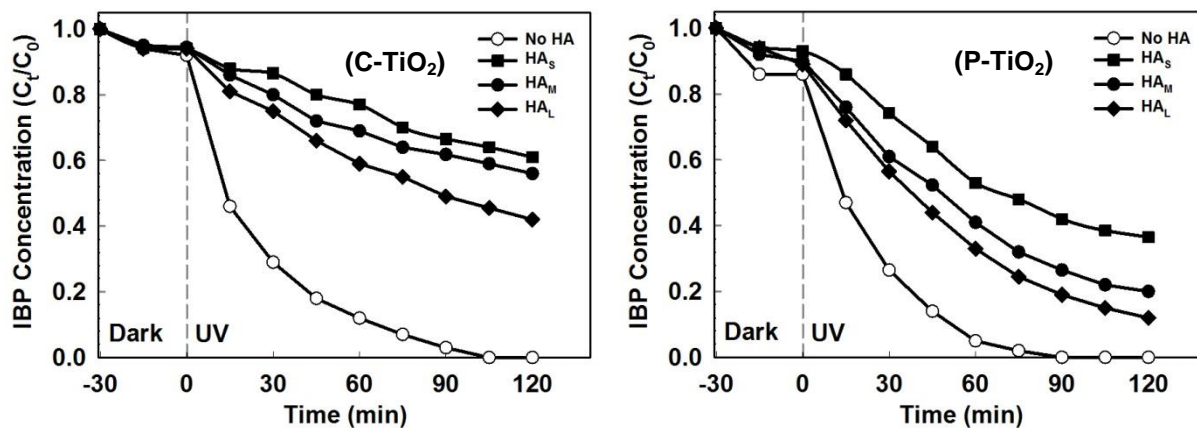
Figure 2.19. Impact of HA size on IBP decomposition and their interaction with porous structure. Larger adverse effect of HA_S on decomposition reaction and effective retention of HA_L using P-TiO_2.

As shown in Figure 2.19, HA_S showed to impose a more significant effect compared to HA_M. In agreement with hypothesis, the small fraction of HA with average molecular size of around 3 nm can freely diffuse within porous structure of $P-TiO_2$, resulting in loss of selectivity. Partial selectivity achieved in this case was a result of greater provided surface area rather than size exclusion mechanism. On the other hand, larger fraction of HA was successfully suppressed by use of $P-TiO_2$.

2.5.7. Discussion on dependability of results

Considering numerous parameters affect the reaction behavior, repeatability of results can be questionable. To evaluate dependability of the results some of the experiments were repeated four times and standard deviation of the results was calculated and visually depicted in Figure 2.20.
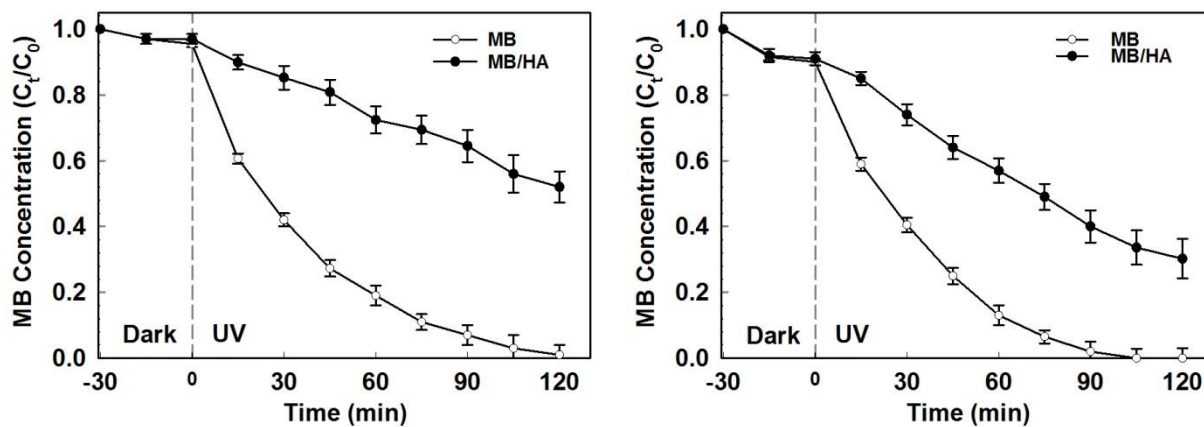
Figure 2.20. Photocatalytic decomposition of MB onto $C-TiO_2$ and $P-TiO_2$

Standard deviation of data points in normalized figures was generally low, limited to 0.026. In order to visually demonstrate the deviations all Std. Dev. Values have been multiplied by a factor of 3 in Figure 2.20. No apparent distinction was observed in repeatability of the results using $P-TiO_2$ and $C-TiO_2$ however both particles show more deviation once HA was introduced to the reaction which can be a result of formation of various intermediates which are very diverse in terms of chemical properties.

34

2.6. Conclusion

There are many studies to demonstrate how the presence of NOM influences target chemical reactions either positively or (mostly) negatively and to control the negative impact of NOM by playing with surface chemistry such as pH adjustment and ionic species addition (Doll and Frimmel, 2005). In this present chapter, we are newly focusing on a physical aspect to achieve the task, i.e., effect of TiO_2 pore size difference on NOM size exclusion to minimize the negative impact of NOM.

All of the results observed in this study well supported the hypothesis on selectivity enhancement by size exclusion on porous TiO_2. The findings of this study can be summarized in following outlines: First, larger size difference between target chemicals and NOM means more effective size exclusion. Second, size of some pores of TiO_2 should be located between sizes of target chemicals and NOM. Pore size of TiO_2 impacts its selectivity and reactivity in various ways. As observed, if pore size becomes close to size of a target chemical, more NOM can be excluded but even a target chemical shows more mass transfer limitation to small pores. This might result in high selectivity towards the target but overall low reactivity. On the other hand, if pore size becomes close to size of NOM, less NOM can be excluded but a target chemical has less mass transfer limitation to large pores. This might result in low selectivity towards the target but overall high reactivity. Considering the opposite effect of relative pore size to sizes of a target chemical and NOM on selectivity and reactivity, optimum pore size is present to balance the tradeoff effect. This might explain why P-TiO_2 photocatalyst exhibited overall better selectivity results in the presence of NOM by balancing between reactivity and selectivity. The relatively large pores of P-TiO_2 can accommodate mass transfer of small target molecules (less than 3 nm) molecules effectively while they can also exclude some of large size NOM molecules properly. It should be noted that pores of TiO_2 have a size distribution rather than having uniform size. Some pores in TiO_2 are large enough for HA to access and the external surface of TiO_2 is always open even to HA. These explain the non-perfect selectivity observed in this case. The principle can also apply to HA with a wide size distribution.

It should be noted that both the chemical interaction and the physical size exclusion between TiO_2 and contaminants are first considered to play an important role in the selective decomposition of

chemicals. In order to focus only on physical aspect of adsorption, same chemical conditions of the reaction solutions (e.g., pH, ionic strength) were applied in all experiments, and the physicochemical properties of the various TiO_2 materials (e.g., crystalline properties and Zeta potential) were proven to be more or less the same except for porous structure. As a result, the observed results can be ascribed exclusively to the structural difference of TiO_2 materials. In summary, an innovative but simple physical approach was developed to increase the selectivity of TiO_2 photocatalysis toward small target contaminants in the presence of macromolecular NOM naturally abundant in water. Size exclusion mechanism of NOM onto porous TiO_2 was investigated by using a set of porous TiO_2 materials and a series of target chemicals and competing chemicals with different sizes. Improved selective decomposition towards small chemicals such as hazardous pharmaceuticals and biological toxins onto porous TiO_2 was achieved by preventing NOM from accessing the catalytic surface mostly available in the porous structure of TiO_2. This study implies the simple size exclusion onto the porous TiO_2 works for selective decomposition of small targets in water containing NOM, unlike previous complex approaches commonly requiring introduction of a secondary material to the TiO_2 surface.

2.7. References

Corin, N.; Backlund, P.; Kulovaara, M. (1996) Degradation products formed during UV-irradiation of humic waters. *Chemosphere*, 33, 245-255.

Doll, T. E.; Frimmel, F. H. (2005) Photocatalytic Degradation of Carbamazepine, Clofibric Acid and Iomeprol with P25 and Hombikat UV100 in the Presence of Natural Organic Matter (NOM) and other Organic Water Constituents. *Water Res.,* 39, 403−411.

Dunn, J. (1996) Algae kills dialysis patients in Brazil Brit. *Med. J.*, 312, 1183–1184.

Keijola, A. M.; Himberg, K.; Esala, A.L.; Sivonen, K.; Hiisvirta, L. (1988) Removal of cyanobacterial toxins in water treatment processes: laboratory and pilot-scale experiments. *Environ. Toxicol.,* 3, 643–656.

Lahti, K.; Hiisvirta, L. (1989) Removal of cyanobacterial toxins in water treatment processes: review of studies conducted in Finland. *Water Supply Manage.,* 7, 149–154.

Lawton, L. A.; Robertson, P. K. J.; Cornish, B. J. P. A.; Jaspars, M. (1999) Detoxification of microcystins (cyanobacterial hepatotoxins) using TiO_2 photocatalytic oxidation. *Environ. Sci. Technol.,* 33, 771–775.

Merel, S.; LeBot, B.; Clément, M.; Seux, R.; Thomas, O. (2009) Ms identification of microcystin-LR chlorination by-products. *Chemosphere,* 74, 832–839.

Nishanthia, S. T.; Rajac, D. H.; Subramanianb, E.; Padiyan, D. P. (2013) Remarkable role of annealing time on anatase phase titania nanotubes and its photoelectrochemical response. *Electrochimica Acta,* 89, 239-245.

Paz, Y. (2006) Preferential Photodegradation-Why and How?. *C.R. Chimie*, 9, 774−787.

Rasoulifard, M.; Fazli, M.; Eskandarian, M. (2014) Degradation of Organophosphorus Pesticide Diazinon Using Activated Persulfate: Optimization of Operational Parameters and Comparative Study by Taguchi's Method. *J. Ind. Eng. Chem.,* 20, 3695−3702.

Volk, C.; Wood, L.; Johnson, B.; Robinson, J.; Zhuc, H. W.; Kapland, L. (2002) Monitoring Dissolved Organic Carbon in Surface and Drinking Waters. *J. Environ. Monit.,* 4, 43−47.

Wen, Z. H.; Chen, L.; Meng, X. Z.; Duan, Y. P.; Zhang, Z. S.; Zeng, E. Y. (2014) Occurrence and human health risk of wastewater-derived pharmaceuticals in a drinking water source for Shanghai, East China., *Sci Total Environ.,* 490, 987-993.

Yu, S-Z. (1994) In toxic cyanobacteria, current status of research and management. *Proceedings of an international workshop,* Australia, D.A. Steffensen, B.C. Nichols (eds.), Australian Centre for Water Quality Research.

Zhang, Z.; Wang, C. C. ; Zakaria, R.; Ying, J. Y. (1998) Role of Particle Size in Nanocrystalline TiO2-Based Photocatalysts. *J. Phys. Chem. B,* 102, 10871−10878.

CHAPTER 3

Effect of pH on TiO$_2$ Surface Charge and Decomposition of Organic Target Contaminants

Heterogeneous decomposition of contaminants using TiO_2 photocatalysts is a promising method for treatment of non-biodegradable water contaminants. TiO_2-based photocatalysis is characterized with non-selective attack to organic compounds which results in significant in decomposition rate of target contaminants when other organic compounds are present in reaction medium. A novel approach for selective decomposition of a variety of target contaminants has been presented herein. A hybrid approach employing electrostatic attraction forces combined with physical separation of organic compounds have been proposed in this study. Engineered meso-porous network of titanium dioxide have been utilized for size-exclusion of competing natural organic matter (NOM) into porous TiO_2 network while electrostatic forces have been employed to facilitate mass transfer of anionic or cationic target contaminants onto active charged surface of TiO_2. Dark condition absorption of anionic Ibuprofen onto positively charged porous TiO_2 showed roughly 2.5 times increase in adsorption capacity compared to non-charged porous TiO_2 In competing condition.

3.1. Introduction

It has been previously stablished that pH plays an important role in the rate photocatalytic decomposition of organic compounds onto TiO_2 photocatalysts. However the previous studies are either focusing on pure reactivity enhancement or their approach to selectivity is based on decomposition of a mixture of compounds onto commercially available non-porous TiO_2 nanoparticles. As a result their proposed approach is generally case sensitive and mostly applicable where target contaminants and competing NOM are very different in terms of ionization state. In real case scenario we are mainly dealing with anionic NOM and also anionic or neutral target contaminants implying methods which are solely based on surface charge can have very limited application. In this chapter we pioneered an approach to simultaneously benefit the size-exclusion as well as enhanced mass transfer induced by electrostatic forces. The selection of medium pH and target contaminants was done based on their pKa and their ionization states. The adsorption capacity and the photocatalytic behavior were correlated with surface charge of TiO_2 and ionic compounds and a distinct trend was observed, evidencing the crucial role of electrostatic forces.

3.2. Material and Methods

Since the separation of material in this part is based on their size and their ionization state, we consider a variety of organic compounds with different pKa values.

Ibuprofen: IBP is an active pharmaceutical ingredient which exist in anionic state at neutral pH. IBP has a reported pKa value in 4.51-4.85 range (Doman´ska et al. 2009) implying that IBP is almost 99% in anionic form at pH 6.5.

Sulfamethoxazole: SMX was used as model target contaminant and similarly to IBP it exists in anionic form at neutral pH. The molecular weight of SMX is approximately 253.28 g mol^{-1} and SMX molecular size was measure by light scattering method to be around 1nm as well. SMX have two pKa values at pKa_1=1.7 and pKa_2=5.5-5.6 (Chen et al.).In this study we only work with pKa_2 since extremely acidic pH could lead to instability of photocatalysts.

Methylene Blue: MB was used as a model cationic organic contaminant. MB has pKa value of 3.8 (kim et al. 2013) implying that at pH above this value it exists mostly in cationic form. The size of MB is more or less similar to IBP and SMX and the variations in its photocatalytic behavior can be attributed to its cationic form and interaction with competing HA.

Humic Acid: HA was used as model NOM and the adsorption of HA to TiO_2 was monitored over pH. HA is reported to have mainly anionic properties (Kam et al. 2001).

3.3. Experimental Setup

Batch reactor was comprised of a cylindrical open top glass reactor placed under two UV lamps emitting peak wavelength of 354nm. The initial volume of each reactor was set to 100 ml and in dark condition adsorption test; the samples were taken out every 15 mins. The TiO_2 nanoparticles were dispersed using sonication prior to experiment. The initial TOC concentrations of HA and IBP, SMX and MB was set to 10 mg l^{-1}. UV intensity at the top of the reactor was measure 3 mW cm^{-2}. The reactor pH was set to 3, 5, 5.5, 6.5 and 10. The pH was stabilized using buffer solution (HPCE buffer solution, Fulka).

3.4. Results and discussions

3.4.1. Surface Charge

Stemmed from Amphoteric characteristics of TiO_2, the precise control of medium pH can be used to induce surface charge. Surface of TiO_2 nanoparticles in water is normally covered with hydroxyl group. As shown in Equation 3.1., this equilibrium could be driven to left hand side (in Acidic Condition) or right hand side (in Basic condition) resulting in protonation and deprotonation of the TiO_2 surface.

$$Ti^{IV}\text{-}H_2 \underset{+H^+}{\overset{-H^+}{\rightleftharpoons}} Ti^{IV}\text{-}OH \underset{+H^+}{\overset{-H^+}{\rightleftharpoons}} Ti^{IV}\text{-}O^- \qquad \textit{Equation 3.1.}$$
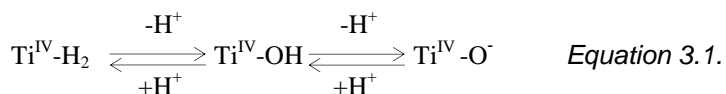
For this sake the Zeta potential of P-TiO_2 and C-TiO_2 material was measure over a variety of pH ranges as presented in Figure 3.1..
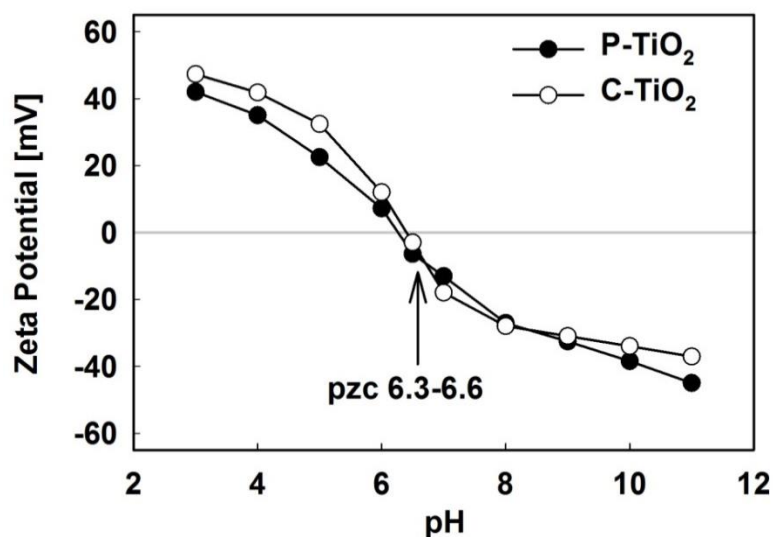
Figure 3.1. Zeta potential of TiO$_2$ surface over pH, both C-TiO$_2$ and P-TiO$_2$ show significant change in surface charge due to protonation and deprotonation caused by acidic condition

In agreement with literature the pzc for TiO$_2$ material falls within 5.5-6.2 pH range. It is also notable the pzc has shifted slightly to left in case of porous TiO$_2$. This effect could be attributed to slight difference in surface affinity toward Hydroxyl group (Preo~anin et al. 2006).   Both catalysts show more or less similar behavior in terms of surface charge. The largest values of + 47mV and -45 mV were observed at pH 3 and pH 11 respectively. We will use pH values of 6.5 to demonstrate neutral surface charge and pH 3 - pH 10 for positive and negative charge accordingly.

3.4.2. Adsorption of Compounds and Effect of pH

Considering short lifetime of reactive hydroxyl radicals, the effective utilization of photocatalysis is closely linked to adsorption of compounds of interest onto active surface of TiO$_2$. In many cases, decomposition reaction takes place though direct interaction of electron/hole with surface bounded contaminants. As proposed in the hypothesis the meso-porous structure of TiO$_2$ with capability to provide internal adsorption sites for target contaminants while rejecting NOM, can potentially increase the selectivity of process.

42

3.4.2.1. Adsorption of IBP

Dark condition adsorption of IBP onto both catalysts, showed significant role of pH-induced surface charge on capacity of TiO_2 in pure adsorption of anionic compounds. Ionization state of the IBP is listed in Table 3.1..

Table 3.1. TiO_2 charge and ionization state of IBP at various pH values

pH	3.0	5.0	5.5	6.5	10
TiO_2 Charge	Positive	Positive	Positive	Neutral	Negative
IBP State	3% Anionic	76% Anionic	90% Anionic	99% Anionic	100% Anionic
Interactions	VW or hydrophobic	Electrostatic	Electrostatic	VW or hydrophobic	VW or hydrophobic

The adsorption behavior of IBP over pH range have been shown in Figure 3.2. As expected from ionization state of IBP, along with increase in TiO_2 positive charge higher adsorption have been observed in both C-TiO_2 and P-TiO_2. However as pH drops below 5, we observe a decline in adsorption of IBP.
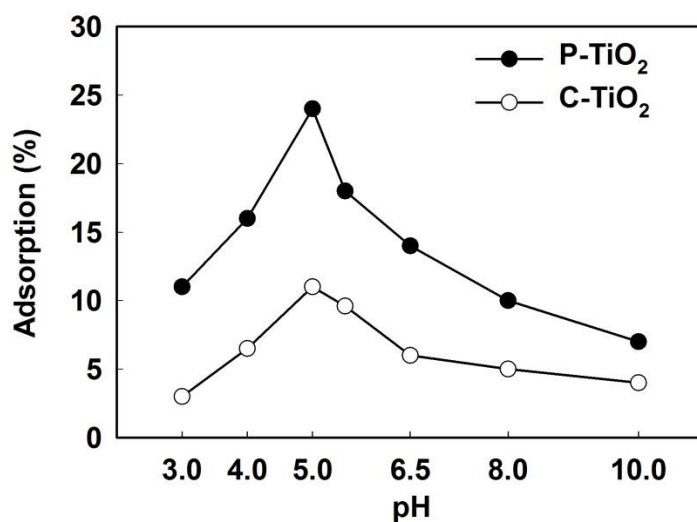
Figure 3.2. Dark Condition Adsorption of IBP onto C-TiO_2 and P-TiO_2

Change in ionization state of IBP could the main reason in this behavior. Since protonation of IBP below pKa (around pH=4.5) leads to formation of neutral molecular form of IBP consequently the affinity of TiO_2 surface for IBP adsorption starts to decline. It should be noted that adsorption in this medium is a complex mixture of wander Waals and Columbus forces and the behavior cannot be explained solely based on charge characteristics of the species.

3.4.2.2. Adsorption of SMX

Similar to IBP, SMX is an anionic compound with slightly higher pKa value. To verify the hypothesis of charge assisted adsorption, we performed the dark condition adsorption around pKa of SMX. It is notable at this point there a tradeoff effect between increased zeta potential and degree of ionization as shown in Figure 3.3..
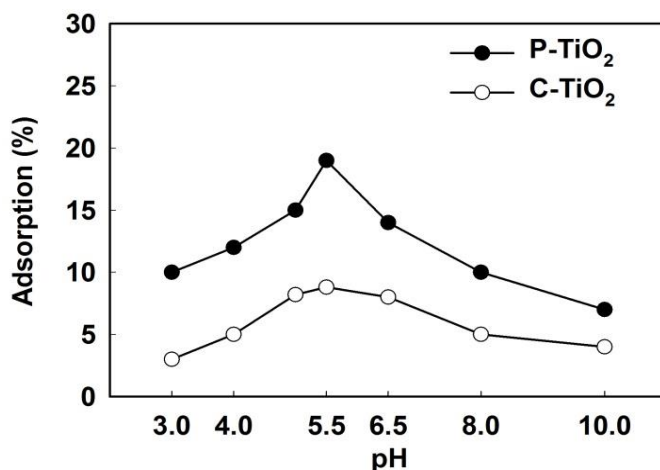
Figure 3.3. Dark Condition Adsorption of SMX onto C-TiO_2 and P-TiO_2

Lower pH is favorable in terms of surface charge while lower pH leads to protonation of anionic SMX and formation of neutral molecules with less affinity for positively charge TiO_2.

Table 3.2. TiO$_2$ charge and ionization state of SMX at various pH values

pH	3.0	5.0	5.5	6.5	10
TiO$_2$ Charge	Positive	Positive	Positive	Neutral	Negative
SMX State	<1% Anionic	25% Anionic	50% Anionic	90% Anionic	100% Anionic
Interactions	VW or hydrophobic	Mostly VW	Electrostatic	VW or hydrophobic	VW or hydrophobic

3.4.2.3. Adsorption of MB

Dark condition adsorption of MB onto both catalysts, demonstrated distinct cationic properties. Ionization state of the MB is listed in Table 3.3..

Table 3.3. TiO$_2$ charge and ionization state of MB at various pH values

pH	3.0	5.0	5.5	6.5	10
TiO$_2$ Charge	Positive	Positive	Positive	Neutral	Negative
MB State	50% Cationic	99% Cationic	100% Cationic	100% Cationic	100% Cationic
Interactions	Electrostatic	Electrostatic	Electrostatic	VW or hydrophobic	Electrostatic

The adsorption of MB over pH range have been shown in Figure 3.2. As expected from ionization state of IBP, along with increase in TiO$_2$ positive charge higher adsorption have been observed in both C-TiO$_2$ and P-TiO$_2$. However as pH drops below 5, we observe a decline in adsorption of IBP.

45
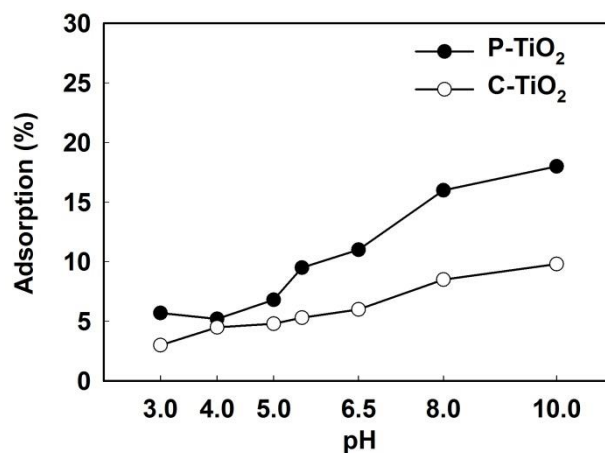
Figure 3.4. Dark Condition Adsorption of MB onto C-TiO$_2$ and P-TiO$_2$

In agreement with mostly cationic properties of MB, an increasing trend in adsorption of MB along with increase in pH was observed.

3.4.2.4. Adsorption of HA onto TiO$_2$

The dark condition adsorption of HA was monitored over various pH. In harmony with literature, the adsorption of HA onto TiO$_2$ follows same behavior as an anionic compound. As shown in Figure 3.5., along with increase in acidity of medium a larger amount of HA is adsorbed onto TiO$_2$.
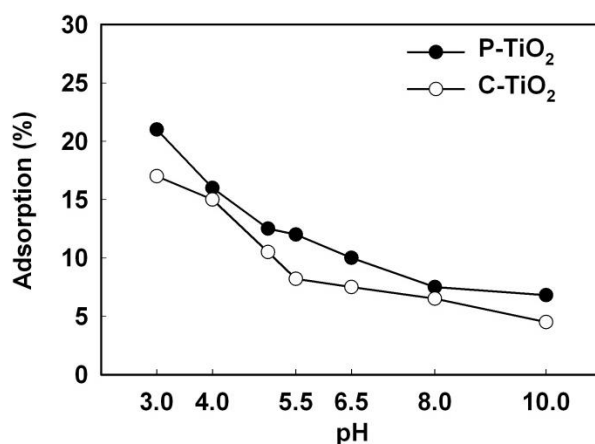
Figure 3.5. Effect of pH on dark condition adsorption of HA. The observed apparent adoption of HA is largely dependent on medium pH.

46

This result can be correlated with Zeta potential of TiO_2 material and the anionic characteristics of HA. The adsorption capacity of P-TiO_2 is slightly larger than C-TiO_2. Interestingly, the adsorption capacity is on average only 20% higher despite the fact that BET surface area is almost 5 times more in P-TiO_2. This result can evidence the size-exclusion role of P-TiO_2.

Table 3.4. TiO_2 charge and ionization state of HA at various pH values

| pH	3.0	5.0	5.5	6.5	10
TiO_2 Charge	Positive	Positive	Positive	Neutral	Negative
HA State	mostly Anionic	mostly Anionic	mostly Anionic	mostly Anionic	mostly Anionic
Interactions	Electrostatic	Electrostatic	Electrostatic	VW or hydrophobic	Electrostatic

3.4.3. Selective Photocatalytic decomposition

3.4.3.1. Effect of pH-induced surface charge on IBP decomposition

In order to assess effectivity of electrostatic forces, four experimental scenarios were designed. In the first scenario the highly ionized IBP was decomposed at pH=6.5 which corresponds to pzc i.e. relatively neutral surface of TiO_2. As shown previously in chapter 2, in this setup P-TiO_2 demonstrated some selectivity mainly due to size-exclusion mechanism. In next scenario the neutral IBP molecules at pH=3 were subjected to photocatalytic decomposition as shown in Figure 3.6.
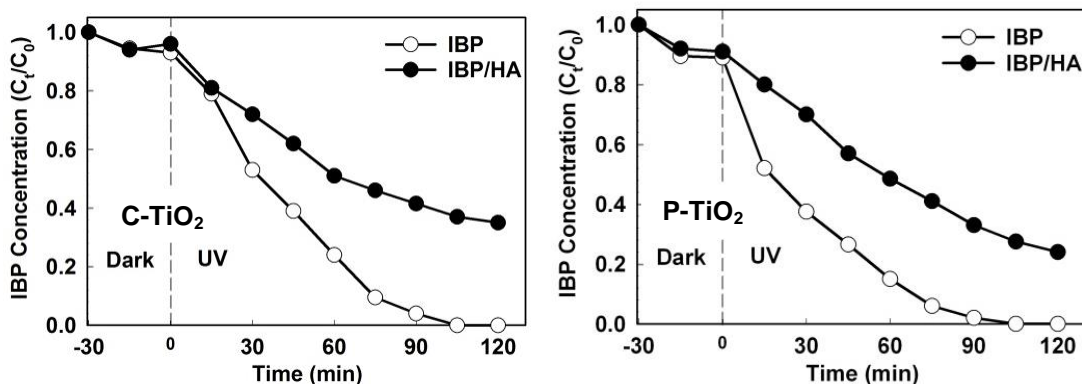
Figure 3.6. Photocatalytic decomposition of IBP at pH=3, based on pKa value of 4.5 most of IBP presents in molecular form at this pH while TiO_2 is positively charged.

The effect of acidic pH on reactivity is generally favorable, the acidic pH generally facilitates generation of OH radicals by providing higher adsorption of OH^- onto TiO_2 surface. As shown in the figure 3.5., the effect of acidic pH in terms of decomposition of IBP in pure condition is rather minimal. This phenomenon could be attributed to molecular form of IBP at this pH. It should be noted that generation of reaction intermediates and their interaction with positively charge TiO2 could be an affecting parameter. Introduction of HA showed to largely affect the photocatalytic decomposition for both $C-TiO_2$ and $P-TiO_2$. In harmony with adsorption curve of HA, we expect the positively charged TiO_2 have adsorbed and decomposed HA in greater degree compared to neutral conditions. Since the pure adsorption of IBP at this pH is relatively low, no meaningful difference can be observed between selectivity of two particles.

Same experiment was repeated at pH=5 (Figure 3.7.).From IBP adsorption curve we expect highest degree of preferential adsorption at this pH. The relatively large surface charge of TiO2 (+22 mV for $P-TiO_2$ and +33 mV for $C-TiO_2$) along with high degree of ionization of IBP facilitates adsorption of IBP onto TiO_2 surface.

48

Figure 3.7. Photocatalytic decomposition of IBP at pH=5, based on pKa value of 4.5 most of IBP presents in anionic form at this pH while TiO_2 is positively charged.

Significantly higher decomposition kinetics of IBP decomposition can be result of electrostatic attraction of IBP onto TiO_2 surface. In competing conditions $C-TiO_2$ shows significant decline compare to pure condition, as a result of competition with anionic HA. Notably the adverse effect of HA introduction was rather small in case of $P-TiO_2$. The difference can be largely due to combined effect of size-exclusion of large HA along with high affinity of positively charged inter-pore surface area for IBP decomposition. It should be noted that selectivity recovery in this case is significantly higher than neutral TiO_2 case, evidencing the role of electrostatic attraction forces in this case.
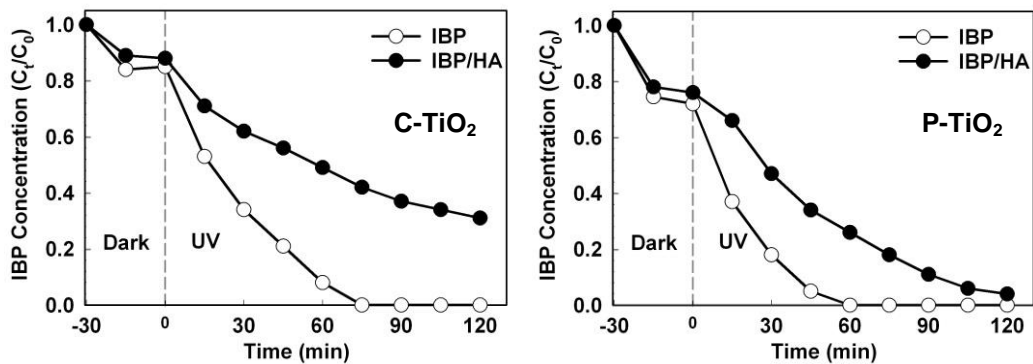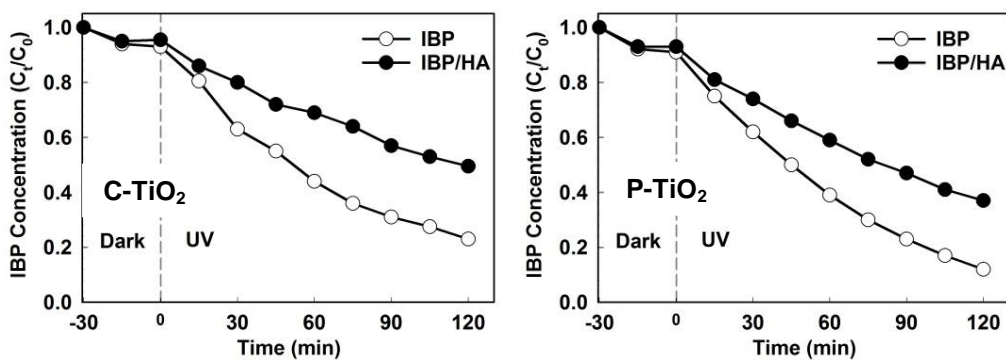

Figure 3.8. Photocatalytic decomposition of IBP at pH=10, based on pKa value of 4.5 most of IBP presents in anionic form at this pH while TiO_2 is negatively charged.

The results from photocatalytic experiment in alkaline condition suggests that even though the adsorption of HA at pH=10 is minimal, the reactivity of TiO_2 toward IBP is minimal (Figure 3.8.), due to less affinity of TiO_2 for IBP adsorption. The repulsion due to negative surface charge and anionic IBP leads to lower adsorption (in dark condition) and consequently lower photocatalytic decomposition rate.

3.4.3.2. Effect of pH-induced surface charge on SMX decomposition

The decomposition of SMX was carried on to distinguish the effect of ionization state on proposed approach. In the first scenario the highly ionized SMX was decomposed at pH=6.5 (corresponding to pzc) as shown in Figure 3.9.

Figure 3.9. Photocatalytic decomposition of SMX at pH=6.5, based on pKa value of 5.5 most of SMX presents in ionic form at this pH while TiO_2 is relatively neutral.

This experimental setup the difference between competing and non-competing performance of particles can be distinguished based on mainly size-exclusion mechanism. The decomposition in pure condition is slightly less than IBP in similar conditions. This could be due to more interfere of reaction intermediates compared to those of IBP. Based on adsorption curve, we repeated the experiment at pH=5.5 where SMX adsorption was at maximum.
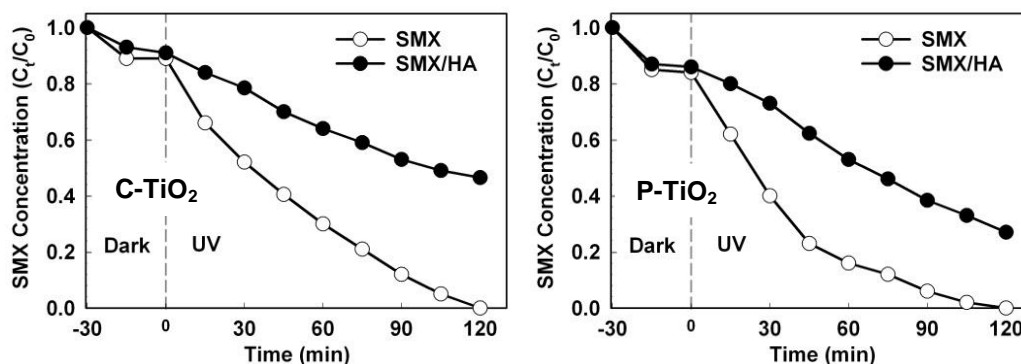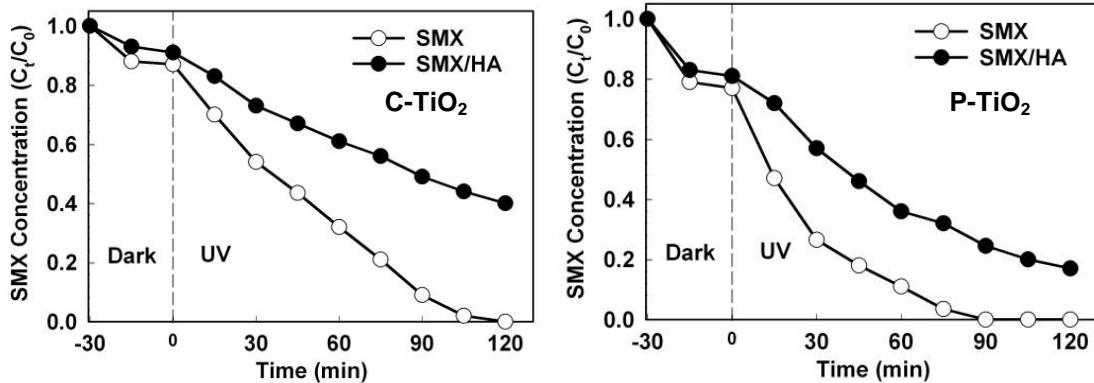
Figure 3.10. Photocatalytic decomposition of SMX at pH=5.5, based on pKa value of 5.5 almost 50% of SMX presents in anionic form at this pH while TiO_2 is positively charged.

Compared to IBP at pH=5, this experimental condition shows less effect on selectivity (Figure 3.10). The lower degree of ionization as well as lower surface charge are possible causes for this observation. Also compared to pH=6.5 we generally have higher HA adsorption which works against the SMX decomposition. However pure condition decomposition shows slight improvement compared to pH=6.5.
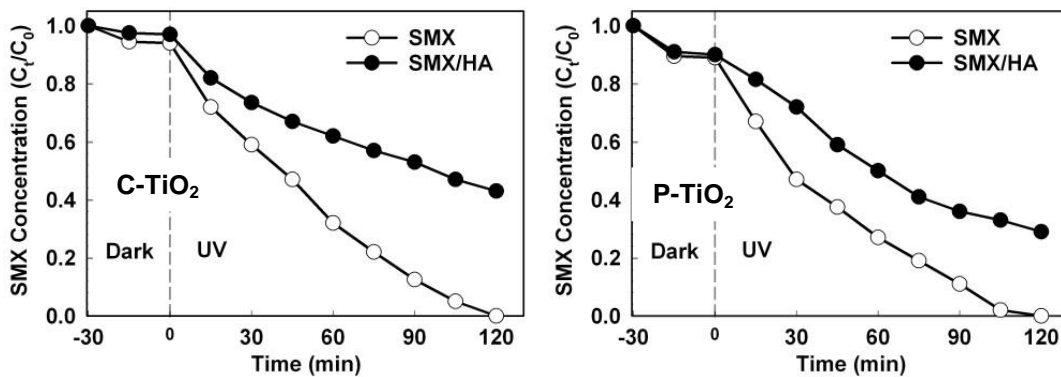
Figure 3.11. Photocatalytic decomposition of SMX at pH=3, most of SMX presents in molecular form at this pH while TiO_2 is positively charged.

51

Similar to IBP, in this case the photocatalytic decomposition shows significant decline along with introduction of HA into reactor.

Along with increase in repulsive electrostatic forces, we can observe the photocatalytic decomposition of SMX shows considerable decline in both C-TiO$_2$ and P-TiO$_2$ as shown in figure 3.12.
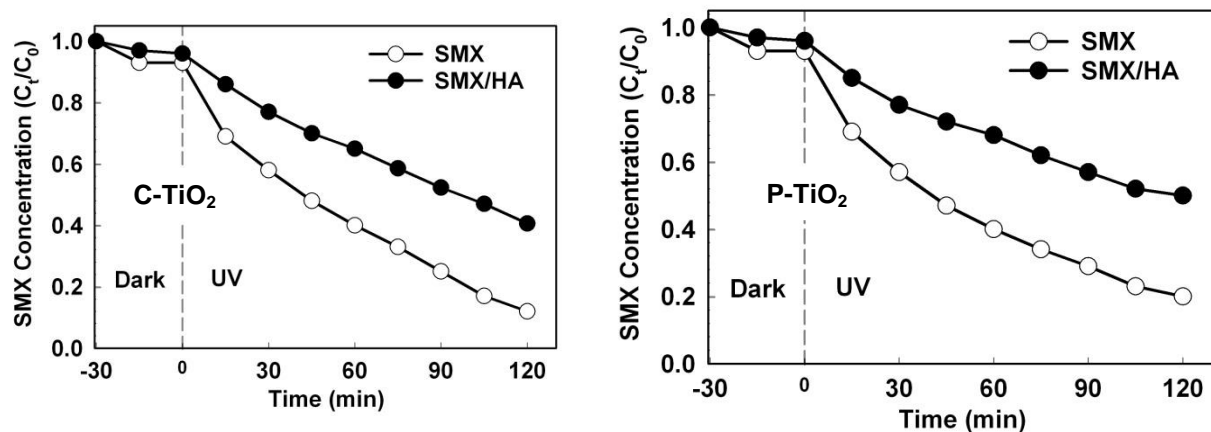
Figure 3.12. Photocatalytic decomposition of SMX at pH=10, most of SMX presents in anionic form at this pH while TiO$_2$ is negatively charged.

3.4.3.3. Effect of pH-induced surface charge on MB decomposition

MB with pKa of 3.1 is consistently cationic over the pH range proposed in this experiment. It have been shown that TiO$_2$ photocatalysts are mainly unstable in extremely acidic pH (below pH 2) and the photocatalytic is concurrent with change in chemical characteristics of TiO$_2$. This effect was avoided by keeping the pH strictly above pH=3 throughout the experiment. The MB decomposition in case of pH=3 was largely affected by adsorption of HA as shown in Figure 3.13.
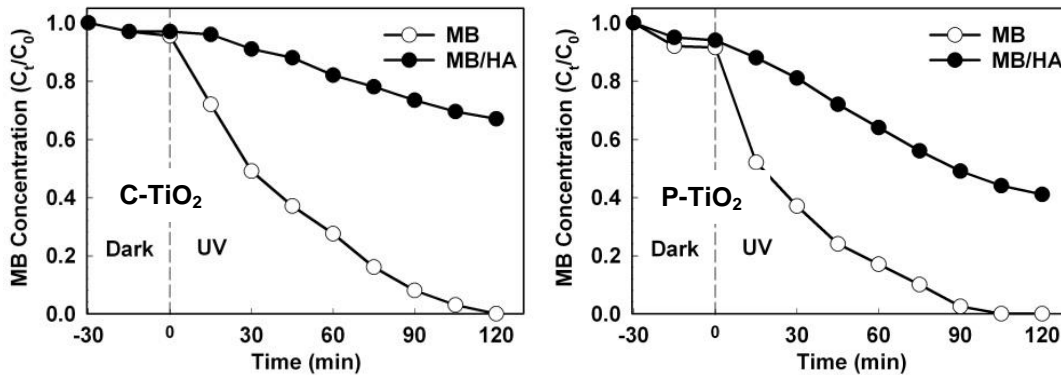
Figure 3.13. Photocatalytic decomposition of MB at pH=3, based on pKa value of 3.1, approximately 50% of MB presents in molecular form at this pH while TiO2 is positively charged (repulsive forces). Anionic HA is largely decomposed at this pH showing the highest adverse effect.

The dark condition adsorption of MB shows the least adsorption due to repulsive forces. Also photocatalytic decomposition exhibits extreme decline compared to pure condition as explained by charge-based attraction/repulsion forces hypothesis. Also the HA adsorption shown to be the highest at this pH.

Figure 3.14. Photocatalytic decomposition of MB at pH=5, MB mainly presents in cationic form at this pH while TiO_2 is positively charged (repulsive forces).

Similarly, the photocatalytic decomposition at pH=5 showed more or less similar results. It is notable P-TiO$_2$ generally showed higher adsorption in both cases. Changing pH from 6.5 to 10 showed the highest impact on selectivity.
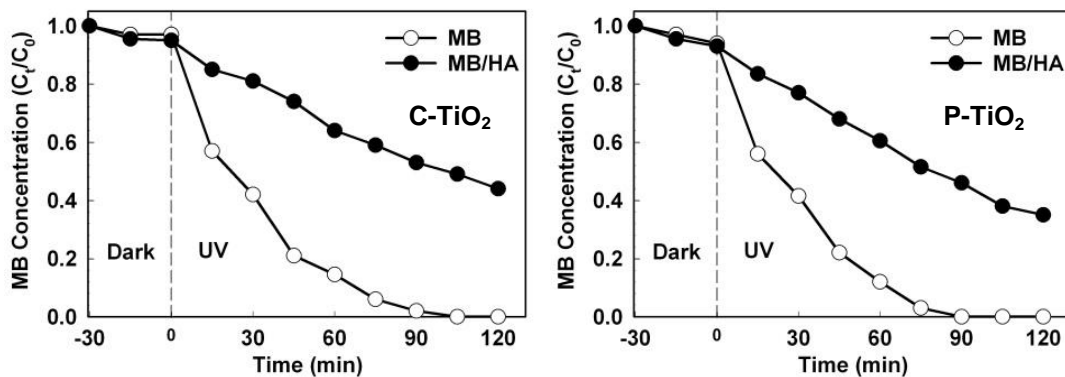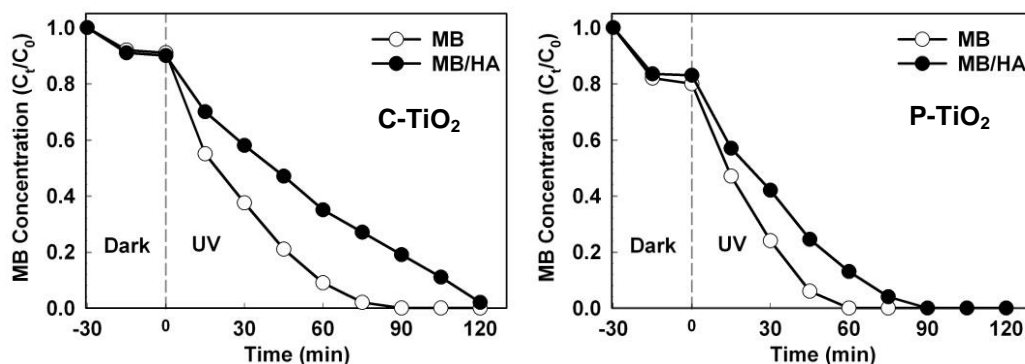

Figure 3.15. Photocatalytic decomposition of MB at pH=10, MB mainly presents in cationic form at this pH while TiO$_2$ is negatively charged (repulsive forces).

The high selectivity can be explained by maximum rejection of HA as well as high affinity toward adsorption of MB at this experimental conditions. Both C-TiO$_2$ and P-TiO$_2$ show relatively high selectivity suggesting that the selectivity enhancement is mainly due to electrostatic interactions in this case rather than size exclusion of species.

Dark condition adsorption of MB and IBP supports the role of inter-pore surface area in adsorption of small size target contaminants as shown in Figures 3.1.- Figure 3.4. However it should be noted, despite significantly large surface area in P-TiO$_2$ compared to C-TiO$_2$ (76.4 m^2 g^{-1} compared to 13.7 m^2 g^{-1}), and the adsorption at pzc was improved marginally (around 85%). This phenomena could be due to competitive adsorption of HA and also due to binding of IBP and MB onto HA instead of TiO$_2$ surface. On the other hand in case of acidic condition significant increase was observed in case of IBP which can be attributed to charge characteristics of P-TiO$_2$ surface providing higher affinity for adsorption of IBP. Similar behavior can be concluded for MB in alkaline condition. HA showed higher affinity to TiO$_2$ surface at acidic conditions as shown in Figure 3.4. while better rejection at alkaline condition. At pH 10, the repulsive forces cause by negatively charged TiO$_2$ and carboxylate ions can effectively decrease the adsorption of HA onto TiO$_2$ surface. The structure of common HA is a rather complex structure comprised

54

of both hydrophobic and hydrophilic functional groups in the carboxyl, phenolic hydroxyl, alcoholic hydroxyl and carbonyl forms (Wiszniowski et al. 2003).

3.5. Conclusion

In summary, a hybrid utilization of size-exclusion mechanism empowered with electrostatic attraction forces, proved to be an effective approach for suppressing the competing decomposition of NOM. Mesoporous structure of titania network provided preferential adsorption sites for decomposition of small size target contaminants while electrostatic forces facilitated the decomposition reaction, by enhancing diffusive mass transfer of ionic target into porous structure. We believe this easy to implement methodology is applicable for a wide variety for selective decomposition of target water contaminants as long as target contaminants and competing NOM, show significant size/charge variation.

3.6. References

Avisara, D.; Horovitz, I.; b, Lozzi, L.; Ruggieri, F.; Baker, M.; Abel, M. L.; Mamane, H. (2013) Impact of water quality on removal of carbamazepine in natural waters by N-doped TiO2 photo-catalytic thin film surfaces. *Journal of Hazardous Materials*, 244–245, 463–471.

Bae, S.; Jung, J.; Lee, W. (2013) The effect of pH and zwitterionic buffers on catalytic nitrate reduction by TiO2-supported bimetallic catalyst. *Chem. Eng. J.,* 232, 327−337.

Cropek, D.; Kemme, P. A.; Makarova, O. V.; Chen, L. X.; Rajh, T. (2008) Selective Photocatalytic Decomposition of Nitrobenzene Using Surface Modified TiO2 Nanoparticles. *J. Phys. Chem. C,* 112, 8311–8318.

Doman´ska, U.; Pobudkowska, A.; Pelczarska, A.; Gierycz, P. (2009) pKa and Solubility of Drugs in Water, Ethanol, and 1-Octanol. *J. Phys. Chem. B.*, 113, 8941–8947.

Inumaru, K.; Murashima, M.; Kasahara, T.; Yamanaka, S. (2004) Enhanced photocatalytic decomposition of 4-nonylphenol by surface-organografted TiO2: a combination of molecular selective adsorption and photocatalysis. *Applied Catalysis B: Environmental,* 52, 275–280.

Lu, X.; Song, C.; Jia, S.; Tong, Z.; Tang, X.; Teng, Y. (2015) Low-temperature selective catalytic reduction of NOX with NH3over cerium and manganese oxides supported on TiO2–graphene. *Chem. Eng. J.*, 260, 776–784.

Preocanin, T.; Kallay, N. (2006) Point of Zero Charge and Surface Charge Density of TiO2 in Aqueous Electrolyte Solution as Obtained by Potentiometric Mass Titration. *CCACAA*, 79, 95-106.

Richardson, S. D.; Ternes, T. A. (2014) Water Analysis: Emerging Contaminants and Current Issues. *Anal. Chem.*, 86, 2813−2848.

Song, L.; Zhu, B.; Gray, S.; Duke, M.; Muthukumaran, S. (2016) Hybrid Processes Combining Photocatalysis and Ceramic Membrane Filtration for Degradation of Humic Acids in Saline Water. *Membranes (Basel),* 6(1):18.

Suttiponparnit, K.; Jiang, J.; Sahu, M.; Suvachittanont, S.; Charinpanitkul, T.; Biswas, P. (2011) Role of Surface Area, Primary Particle Size, and Crystal Phase on Titanium Dioxide Nanoparticle Dispersion Properties, *Nanoscale Res Lett,* 6:27.

Volk, C.; Wood, L.; Johnson, B.; Robinson, J.; Zhuc, H. W.; Kapland, L. (2002) Monitoring dissolved organic carbon in surface and drinking waters. *J. Environ. Monit.,* 4, 43−47.

Wiszniowski, J.; Robert, D.; Surmacz-Gorska, J.; Miksch, K.; Weber, J. V. (2003) Photocatalytic mineralization of humic acids with TiO2:Effect of pH, sulfate and chloride anions. *International Journal of Photoenergy,* 5, 69-74.

Yamamoto, A.; Mizuno, Y.; Teramura, K.; Shishido, T.; Tanaka, T. (2013) Effects of reaction temperature on the photocatalytic activity of photo-SCR of NO with NH3 over a TiO2 photocatalyst. *Catal. Sci. Technol.*, 3, 1771−1775.

Yoneyama, H.; Haga, S.; Yamanaka, S. (1989) Photocatalytic activities of microcrystalline TiO2 incorporated in sheet silicates of clay. *J. Phys. Chem.,* 93, 4833−4837.

Zakersalehi, A.; Nadagouda, M.; Choi, H. (2013) Suppressing NOM Access to Controlled Porous TiO2 Particles Enhances the Decomposition of Target Water Contaminants. *Catal. Comm,* 41, 79−82.

CHAPTER 4

Recommendations and Potential Applications

4.1. Recommendations

This study aimed at presenting two general approaches to address the issue of lack of selective photocatalytic decomposition in crystalline TiO_2 material with focus on water treatment applications. The results from various compounds evidenced the crucial role of porous structure in governing the photocatalytic behavior of TiO_2. Although the results are based on specific target contaminants, the presented mythology could be utilized to address a wider range of chemicals. Specially presented modified sol-gel method can be modified to optimize the process for each case. Future work should be done to focus on scale-up issues.

4.1.1. Synthesis of meso-porous TiO$_2$ with narrow pore size distribution

The efficiency of size-exclusion mechanism is largely dependent on pore size distribution ad well as spatial configuration of TiO_2 porous network. As demonstrated in chapter 2 and chapter 3, porous TiO_2 with extremely high BET surface area can be simply synthesized by modifying sol-gel method with surfactant addition. However not all inter porous surface area was utilized as demonstrated in adsorption result. Further studies with aim to manipulate the porous structure of the TiO_2 with the following aim can enhance the applicability and performance of this approach:

- Synthesis of porous TiO_2 with narrow pore size distribution
- Enhancing diffusive mass transfer of target contaminants

4.1.2. Synthesis of charged crystalline TiO$_2$

Generation of surface charge was directly related to amphoteric properties of TiO_2 and thus pH adjustment was required in order to achieve surface charge. However in real case the medium pH is not a parameter of choice. Also the pH adjustment in scale of water treatment facility is technical and economically not practical. It have been previously stablished that modification of sol-gel method with charged species can result in charged surface of synthesized TiO_2 (Nelson et al. 1999, Kim et al. 2015). However most of these methods are based on low temperature synthesis pf TiO_2 which suggests that

synthesized TiO_2 lacks high crystallinity and thus low reactivity. Utilization of new low temperature synthesis routes for fabrication of porous crystalline TiO_2 with charge characteristic as an inherent part of photocatalyst can be of great benefit for selective decomposition of target contaminants without changing the reaction parameters.

4.2. Potential Applications

Despite many alternative treatment technologies, of TiO_2 –based systems (in general photocatalytic systems) are capable of complete destruction of toxic contaminants. Most of the current filtration and adsorption methods are simply based on phase transfer of contaminants from one medium to another. This property of TiO2 can be utilized specially in places where closed system requires decomposition of contaminants.

4.2.1. Photocatalytic ceramic membrane

It should be noted that utilization of TiO2 is far beyond solely photocatalysis. The applications of TiO_2 as tunable "photocatalytic ceramic membrane" opens a new horizon in applications of this technology. The presented tailor-designing method can be used to fabricate TiO_2 material in shape of single or multi-layer membranes. Interestingly multi-layer membrane with narrow small pores in surface and highly porous structure in support layer can achieve a robust, yet very size selective configuration (Zakersalehi et al. 2013). This membrane by utilizing photocatalytic characteristics, can resolve the fouling problem which is believed to be the main drawback of filtration system (Nguyen et al. 2012). They are also very effective in regards to disinfection and visible light activation. The concurrent decomposition properties along with precise molecular sieving effect can revolutionaries this industry. The module is especially superior in terms of continuous treatment capability as long as supply of irradiation energy is provided. Continuous treatment and recycle of water is highly attractive for remote places with limited water availability.

4.2.2. Photocatalytic decomposition of biological toxins

As demonstrated in chapter 2 and chapter 3, MC-LR can be effectively removed from water resources by mean of TiO_2 photocatalysis. MC-LR is mainly released as a result of hazardous algal bloom in lakes or places with large concentration of NOM. The proposed size exclusion mechanism can be utilized to selectively address this issue while minimizing interactions with NOM.

4.3. References

Kim, S.; Sinai, O.; Lee, C. W.; Rappe, A.M. (2015) Controlling oxide surface dipole and reactivity with intrinsic nonstoichiometric epitaxial reconstructions, *PHYSICAL REVIEW B*, 92, 235431

Nelson, B. P.; Candal, R.; Corn, R. M.; Anderson, M. A. (2000) Control of Surface and ú Potentials on Nanoporous TiO_2 Films by Potential-Determining and Specifically Adsorbed Ions, *Langmuir*, 16, 6094-6101.

Nguyen, T.; Felicity, Roddick, A.; Fan, L. (2012) Biofouling of Water Treatment Membranes: A Review of the Underlying Causes, Monitoring Techniques and Control Measures, *Membranes*, 2, 804-840.

Zakersalehi, A.; Choi, H.; Andersen, J.; Dionysiou, D. D. *Photocatalytic ceramic membranes*

Hoek, E. M. V.; Tarabara, V.V. (2013) Encyclopedia of Membrane Science and Technology, *John Wiley & Sons*

Biographical Information

Abolfazl Zakersalehi obtained his BS degree in Civil Engineering at Sharif University of Technology In Tehran. He pursued his academic and professional interests further with a MS degree in Environmental Engineering at the University of Texas at Arlington. As part of his MS degree, he investigated the selective decomposition of Ibuprofen onto TiO_2 photocatalysts. He enrolled as a Ph.D. student in Civil Engineering at the University of Texas at Arlington in August 2013 and he investigated novel approaches to address the selectivity issue in TiO_2 photocatalysts. His research has been presented in several national and international conferences. From his Ph.D. research studies, he has submitted two research articles. He is also co-author of two book chapters focusing on practical applications of photocatalysis technology for water treatment. Mr. Zakersalehi long term professional goal is to secure a research position in an industrial research and development institution where he can utilize research in the field of environmental engineering to contribute towards providing a sustainable environment.